LAWRENCE
LIVERMORE
NATIONAL
LABORATORY

UCRL-JRNL-206367

Evaporative Evolution of a Na-Cl-NO3-K-Ca-SO4-Mg-Si Brine at 95(degree)C: Experiments and Modeling relevant to Yucca Mountain, Nevada, USA

M. Alai, M. Sutton, S. A. Carroll

September 3, 2004

Geochemical Transactions

UCRL-JRNL-206367

Evaporative Evolution of a Na-Cl-NO_3-K-Ca-SO_4-Mg-Si Brine at 95°C: Experiments and Modeling relevant to Yucca Mountain, Nevada, USA

Maureen Alai*, Mark Sutton, and Susan Carroll

Lawrence Livermore National Laboratory, Livermore, CA 94550, USA

***Corresponding author**

E-mail address: alai1@llnl.gov (M. Alai)

Abstract

A synthetic Topopah Spring Tuff water representative of one type of pore water at Yucca Mountain, Nevada (USA) was evaporated at 95ºC in a series of experiments to determine the geochemical controls for brines that may form on, and possibly impact upon the long-term integrity of waste containers and drip shields at the designated high-level, nuclear-waste repository. Solution chemistry, condensed vapor chemistry, and precipitate mineralogy were used to identify important chemical divides and to validate geochemical calculations of evaporating water chemistry using a high temperature Pitzer thermodynamic database.

The water evolved towards a complex "sulfate type" brine that contained about 45 mol% Na, 40 mol% Cl, 9 mol% NO_3, 5 mol% K, and less than 1 mol% each of SO_4, Ca, Mg, $\sum CO_2$(aq), F, and Si. All measured ions in the condensed vapor phase were below detection limits. The mineral precipitates identified were halite, anhydrite, bassanite, niter and nitratine. Trends in the solution composition and identification of $CaSO_4$ solids suggest that fluorite, carbonate, sulfate, and magnesium-silicate precipitation control the aqueous solution composition of sulfate type waters by removing fluoride, calcium, and magnesium during the early stages of evaporation. In most cases, the high temperature Pitzer database, used by EQ3/6 geochemical code, sufficiently predicts water composition and mineral precipitation during evaporation. Predicted solution compositions are generally within a factor of two of the experimental values. The model predicts that sepiolite, bassanite, amorphous silica, calcite, halite and brucite are the solubility controlling mineral phases.

1.0 INTRODUCTION

Yucca Mountain, Nevada, USA is the designated site for a permanent geologic repository for high-level nuclear waste in the USA. The current waste package design consists of a double walled container with an inner barrier of stainless steel, an outer barrier of highly corrosion resistant nickel-chromium-molybdenum alloy, and a titanium alloy drip-shield that covers the containers. Corrosion resistance and long-term integrity of the metal containers and shields are important for the safe disposal of the waste. Characterization of the compositional evolution of waters that affect waste package corrosion is necessary. If the site is licensed, the waste packages will be placed in tunnels several hundred meters below the ground surface and above the groundwater table in partially saturated volcanic tuff. Once the waste packages are in place, the repository will heat up due to the thermal energy of the nuclear waste. Although the waste packages will be above the groundwater table, pore water present in rock formations within (Topopah Spring Tuff) and above (Paintbrush Tuff) the repository may come into contact with the metal containers and shields. Additionally, brines may form from the deliquescence of salts found in dusts deposited on the containers.[1] In this study we focus on seepage brines formed by the evaporation of pore water at elevated temperature.

One method of evaluating the evolution of a brine is the chemical divide theory, which has been used to describe saline lake geochemistry.[2-5] The chemical divide theory generally describes the chemical evolution of dilute waters upon evaporation in terms of their equivalent calcium, sulfate and bicarbonate ratios and is shown in Figure 1a. The chemical evolution of evaporating water is controlled by the high solubility of salt minerals relative to the moderate solubility of calcium sulfate and low solubility of calcium carbonate minerals. A bicarbonate alkaline brine (Na-K-**CO_3**-Cl-SO_4-NO_3) forms from dilute waters with dissolved calcium concentrations that are less than dissolved carbonate ($Ca < HCO_3+CO_3$, equivalent %). A sulfate brine with near neutral pH (Na-K-Mg-Cl-**SO_4**-NO_3) forms from dilute waters with dissolved calcium concentrations that are greater than the dissolved carbonate, but less than the combined dissolved sulfate and carbonate concentrations ($Ca < SO_4+HCO_3$, equivalent %). A calcium chloride brine with near neutral pH (Na-K-**Ca**-Mg-Cl-NO_3) forms from dilute waters with a dissolved calcium concentration that is greater than the combined dissolved sulfate and carbonate concentrations ($Ca > SO_4+HCO_3$, equivalent %). The measured compositions of Yucca Mountain pore water vary, but can be generally classified as waters that should evolve towards sulfate and sodium bicarbonate type brines, with a few calcium chloride brines as they evaporate (Figure 1b).[6-8]

In Figure 1, the simple ratios of calcium, sulfate and carbonate illustrate the dominant carbonate and sulfate chemical divides that occur as waters evaporate.[2,9,10] However, Figure 1 does not show important chemical divides for magnesium, silica, or fluoride, nor does it show the relative amount of these salts to other major ions such as sodium, chloride and nitrate. These are important chemical parameters, because they may mitigate or enhance the corrosiveness of brines at the waste package surfaces. Temperature will also impact the evolution of the pore water. Previous modeling of Yucca Mountain pore water initially within the sulfate brine field at

25ºC evolved towards calcium chloride brines at 95ºC, and not towards a sulfate brine as predicted by Figure 1a.[7]

Thermodynamic equilibrium codes use a range of seepage water chemistry, temperature and relative humidity to model the chemical environment on Yucca Mountain waste package surfaces.[1] This requires Pitzer parameters that can account for non-ideal solutions at higher ionic strengths and elevated temperatures. Unfortunately, only a few relevant experiments are available to validate this modeling approach. The available data consists of evaporation of two bicarbonate type waters modeled after Yucca Mountain J-13 well water and a calcium chloride type water modeled after unsaturated pore water at Yucca Mountain and seawater.[1, 5]

In this paper we focus on the brine chemistry formed by the evaporation of a synthetic Yucca Mountain sulfate type pore water[8] at 95ºC over a concentration range of 1x to ~3500x. This study provides additional benchmark data needed to both understand the brines and salts that form upon evaporation of various waters and to validate the EQ3/6 geochemical code and a high temperature Pitzer parameter thermodynamic database currently used by the Yucca Mountain Program to model aqueous chemical systems.

2.0 METHODS

2.1 Experimental Methods

A synthetic pore water solution, based on HD-PERM-1 pore water composition[8], was evaporated about 3400 times at 95ºC in a series of experiments to iteratively concentrate the solution in manageable quantities of approximately 2 liters and to monitor precipitation. The chemical composition of each successive leg was based on the brine composition towards the end of the previous leg (Table 1). Experiments FEC 9, 12, 13, and 14 are referred to as legs 1, 2, 3, and 4 throughout this paper. The solutions were prepared at room temperature using analytical grade salts. Differences between the ending and starting compositions for each leg reflect the difficulty in exactly synthesizing the solutions and changes that occur when the solution is prepared at 25ºC and then heated to the experimental temperature of 95ºC. At the beginning of each new leg, the prepared solution did not include the undissolved solids that were present at the end of the previous leg. During the preparation of the starting solution for legs 3 and 4, an amorphous magnesium silicate precipitate formed in the 25ºC solutions. This precipitate was not removed from the starting solutions and only partially dissolved when the solution was heated up to the experimental run temperature (95ºC).

Evaporation was conducted in a vented, halar-lined vessel heated to 95ºC in a fluidized sand bath furnace which provided optimal heat transfer for this method. The solution was stirred constantly and HEPA (High Efficiency Particulate Air) filtered air was streamed over the solution to help control the evaporation rate. The solution vapor was refluxed to prevent evaporative water loss as it was heated to run temperature. Once the solution was at 95ºC, the evolving water vapor was condensed into a separate container to monitor the extent of evaporation. Samples of the evaporating solution were periodically extracted and filtered at 95ºC and analyzed to determine the water chemistry. The 95ºC filtered samples withdrawn for cation and anion analysis were immediately diluted by directly injecting the sample into a known quantity of room temperature deionized water to prevent precipitation on cooling. Undiluted

samples withdrawn for total dissolved inorganic carbon analysis, $\sum CO_2(aq)$, were immediately stored by filling gas tight vials to prevent equilibration with air at room temperature. Separate undiluted samples for solution pH were stored in a closed container and pH was measured as soon as they cooled to room temperature. In the last two samples of leg 4, precipitates formed in the pH and carbon samples as they cooled. Samples of the condensed water vapor were also periodically extracted and analyzed to monitor gas volatility. After the last sample was taken for each leg, the evaporation was continued to dryness. The solid precipitate was collected at the end of each leg of the experiment, dried in an oven at 40ºC to facilitate sample preparation, and analyzed by powder X-ray diffraction (XRD).

2.2 Analytical Methods

Sample pH was measured at room temperature with a combination electrode, which is reliable in solutions with an ionic strength less than 0.1 molal.[11] The sample cooled to room temperature and pH was measured within a half hour of sampling. The pH measurements for legs 3 and 4, where the ionic strength of the solution was greater than 0.1 molal, represent uncorrected values and have not been corrected for ionic strength. Total dissolved carbon, $\sum CO_2(aq)$, was measured with an infrared carbon analyzer and had a detection limit of 1 ppm. Dissolved calcium, magnesium, silica, and sodium were measured with an inductively coupled plasma-atomic emission spectrometer, dissolved potassium was measured using an atomic absorption spectrophotometer, and fluoride, chloride, nitrate, and sulfate anions were determined using ion chromatography. Reproducibility of these techniques is typically better than ±2%. The mineralogical composition was determined by powdered X-ray diffraction (XRD) using a Cu-K-alpha source from 10º to 90º 2-theta at 0.02º per step. The XRD instrument was calibrated using NIST traceable silicon (# 640c) and mica (# 675) standards for high angle and low angle peaks, respectively. XRD cannot detect amorphous solids or minerals that are present at < 2 wt %. Mineral identification was based on the presence of the three most intense peaks in the XRD pattern for a given mineral. In some cases where the most intense peaks overlapped with other mineral peaks, identification was based on the presence of lower intensity diagnostic peaks.

2.3 Thermodynamic Modeling Calculations

Solution compositions were modeled using the EQ3/6 geochemical code, and a high temperature Pitzer ion-interaction model that is further described in Appendix 1.[1, 12-14] The high temperature Pitzer ion-interaction model approximates non-ideal behavior of solutions at elevated ionic strength and temperature. The predictive models were generated to mirror the experimental design and analysis, in which synthetic pore water was evaporated over a discrete range for each leg, with a cumulative evaporation up to 3500x for the overall experiment. The concentration factor, CF, can then be defined as:

$$CF_{(n)} = \frac{H_2O_{(i)}}{H_2O_{(n)}} \qquad 1.$$

where $H_2O_{(i)}$ is the initial mass of H_2O solvent and $H_2O_{(n)}$ is the mass of H_2O solvent remaining after the n^{th} step in the evaporation process.

The evaporation model consisted of three steps. In the first step, the measured composition of the first sample at 95°C (Table 1, FEC#-1) was speciated, suppressing all mineral precipitation in the calculation. At this point in the experiment, the solution was simply brought up to temperature, refluxing any water vapor to prevent evaporation. During the second step, the speciated water was evaporated by stepwise removal of solvent water at a fixed rate of 0.25 mol H_2O reactant per mol of solute at 95°C. In the evaporation step, all minerals were allowed to precipitate with the exception of quartz and dolomite because of known slow kinetics; glaserite, hydromagnesite and magnesite because the available thermodynamic data are questionable; and cristobalite because it forms above 1470°C and is not relevant to this experiment. In the speciation and evaporation steps, oxygen and carbon dioxide fugacities were fixed at 21% and 0.033% respectively to simulate atmospheric experimental conditions. A CO_2(g)-sink was added to the model to remove excess buildup of CO_2(g) from the reaction surface. Finally, in the third step, the predicted pH values at 95°C were recalculated to 25°C to compare with measured pH at room temperature. This was achieved by performing a further calculation that reduced the temperature of the reaction from 95°C to 25°C, while fixing $\sum CO_2$(aq) to the predicted 95°C value and suppressing mineral formation. For all calculations, electrical balance was achieved by automatically changing the sodium concentration with a convergence tolerance of 0.1ppb. Charge balancing was necessary due to analytical errors generated in the experimental analysis and also potentially incomplete analysis. The calculated activity of water was interpreted as a function of relative humidity, and predicted solution composition, pH and mineral composition were compared with experimental ion analysis and XRPD results with respect to the overall concentration factor. The results are shown graphically in Figures 3 and 4, and discussed in the following sections.

3.0 RESULTS

Evaporation of the dilute water yielded a sulfate brine as predicted by chemical divide theory based on its initial $Ca:SO_4:HCO_3$ ratio (Figure 2). Although this water is classified as a sulfate brine, sulfate concentrations are minor compared to the concentration of sodium and chloride, which dominate the solution chemistry. At the conclusion of leg 4, sodium and chloride were 45 and 40 mol% respectively while calcium and sulfate were relatively minor constituents at 0.1 and 0.8 mol% respectively (Table 2). The initial experimental solution contained trace amounts of fluoride that were rapidly removed from solution presumably as highly insoluble fluorite (CaF_2) (Table 1). Fluoride was not included in the model since it was not detected in the first sample analysis at 95°C (leg 1, FEC9-1). The minerals identified by XRD in the precipitates are halite (NaCl), bassanite ($2CaSO_4 \cdot H_2O$), anhydrite ($CaSO_4$), niter (KNO_3), and nitratine ($NaNO_3$), and are listed for each leg in Table 3.

We see no evidence of volatility for HCl, HNO_3, and HF gases in these experiments. Concentrations of fluoride, chloride, nitrate and sulfate in the condensed vapor were all below the detection limits. This is in contrast to evaporation of a concentrated calcium chloride type

water at around 140ºC (based on the 1000x solution results from Rosenberg et al[5]) where significant volatilization of HCl(g) was measured by acidic condensates at 90% evaporation at ~75,000x.[15] While our evaporation is less than the aforementioned research, our results indicate that gas volatility is not a major concern for the evaporation and concentration of sulfate waters at 95ºC and ~3,400x.

Figures 3 and 4 show the experimental and predicted solution composition and the predicted mineral precipitation as a function of overall concentration factor. There is excellent agreement between the model predictions of potassium and nitrate concentrations with those measured by experiment. Solution data show conservative concentration of both potassium and nitrate in each evaporation leg, indicating no mineral precipitation (Figure 3a & 4). This is supported by the XRD data where only a small amount of niter was identified in the last leg after the solution had completely evaporated when precipitation of all mineral phases is expected (Table 3). Calculations required the suppression of pentasalt (gorgeyite, $K_2Ca_5(SO_4)_6 \bullet H_2O$) precipitation at a concentration factor above 1000x in leg 4 (Figure 3a) to achieve agreement with experimental solution composition and solid characterization. Pentasalt was not detected by XRD analysis.

For sodium and chloride behavior, we observe good agreement between experimental composition and model prediction (Figure 3b & 4). Both ions concentrate in solution with increasing evaporation until the solution is saturated with respect to halite. Halite is the dominant salt in samples taken to dryness and identified by XRD (Table 3). There is a discrepancy between the experimental sodium concentration and that predicted by the model in leg 1, due to the charge balance correction using sodium ions in the model. This observation is explained by the over-prediction of positively charged magnesium, and the subsequent decrease in calculated sodium concentration to neutralize the charge discrepancy. The charge balance correction resulted in a sodium concentration that differed from the original (measured) concentration by 21% in the first leg, 13% in the second leg, 1% in the third leg and 5 % in the fourth leg. Since sodium saturation did not occur until the formation of halite late in fourth leg, we believe this sodium correction did not significantly affect the quality of our calculations.

There is also good agreement between experimental compositions and model prediction for calcium and sulfate (Figure 3c & 4). At a concentration factor of roughly 10x in leg 2, both calcium and sulfate begin to precipitate as can be seen in the decrease in their slopes. Although calcium sulfate precipitation continues over the duration of the experiment, dissolved calcium decreases as the sulfate increases with continued evaporation at a concentration factor of about 1000x. This is consistent with the chemical divide theory and the initial composition of the water which contained SO_4:Ca > 1. This behavior was best modeled by using bassanite as the solubility limiting phase (using gypsum or anhydrite resulted in an over-prediction and under-prediction respectively of the calcium and sulfate concentrations). This finding is in partial agreement with the experiments, which identified both anhydrite and bassanite (Table 3). This difference may be an artifact of the experimental protocol because calcium sulfate hydration states can be readily altered by changes in temperature and humidity, such as those found in the drying and preparation of the precipitate prior to XRD analysis. The model over-estimates calcium and sulfate by about a factor of two in concentrated brines (1000x concentration factor), and appears to increase with continued evaporation. It is possible that the over-prediction in

calcium and sulfate concentrations observed using bassanite and gypsum solubility controls, and the under-prediction observed with anhydrite controls indicates a metastable mixture of these solubility limiting phases.

Comparison between both magnesium and silica experimental concentrations and model predictions during the evaporation show reasonable agreement in legs 2 and 3 and only fair agreement in legs 1 and 4 (Figure 3f). Experiment and prediction both show that magnesium and silica are removed from solution as solid precipitates. The model predicts that sepiolite, amorphous silica, and brucite are the solubility controls (Figure 4). These phases were not observed in the experiment possibly because the amount was too small to be detected or because they were amorphous. It is possible that a non-crystalline magnesium silicate phase precipitated, similar to the solid that formed at 25ºC (Legs 3 and 4).[16] The Pitzer database contained only two magnesium silicate minerals, talc ($Mg_3Si_4O_{10}(OH)_2$) and sepiolite ($Mg_4Si_6O_{15}(OH)_2 \cdot 6H_2O$). A better model fit was achieved when sepiolite was allowed to precipitate and talc formation was suppressed.

There is good agreement between the experimental and predicted total dissolved carbonate in the final leg (shown in Figure 3d as $\sum CO_2(aq)$), assuming equilibrium with atmospheric $CO_2(g)$ at temperature. In more dilute legs 1 to 3, total dissolved carbonate was not detected after the first few samples for each leg. Predicted carbonate concentrations for legs 1, 2 and 3 are all below the detection limit and are consistent with the experiment. The failure of the model to capture the initial dissolved carbonate concentrations suggests that $\sum CO_2(aq)$ in starting solution synthesized at 25ºC had not degassed to the lower equilibrium amount at 95ºC. Model predictions show that carbonate concentrations decrease throughout the evaporation process as carbonate is lost to the atmosphere as gaseous CO_2 in conjunction with a decreasing pH. No carbonate minerals were predicted to form until leg 4, where a very small amount of calcite precipitates, which was too small to be detected by XRD.

Model prediction of pH in the first two legs is in reasonable agreement with experimental data showing that the pH values decrease during the evaporation in each leg (Figure 3e). However, in legs 3 and 4 where the ionic strength exceeds 0.1 molal, measured pH values are uncorrected and are as much as 2 pH units lower than the predicted pH. The measured values were not corrected for ionic strength effects in these complex solutions. Rai and Felmy[17] report that measured pH will be lower than the actual pH by 0.14 units in 1 molal NaCl and by 0.97 pH in 6 molal NaCl due to the ionic strength effects on the liquid junction potential of a commercially available 3 M KCl combination electrode similar to that used in these experiments. Even larger discrepancies between measured and real pH values are seen in more complex systems containing mixtures of mono and divalent ions at high ionic strength. The difference in measured pH at the end of one leg and the start of the next leg is an artifact of the experimental protocol. The waters were synthesized at room temperature, equilibrated with atmospheric $CO_2(g)$ and have higher dissolved carbon and higher pH than they possess at 95ºC.

Accurate prediction of pH is very important because the solubility of many solid phases, such as sepiolite, calcite, and amorphous silica are strongly influenced by solution pH. Therefore, it is possible that the discrepancy between experimental and predicted values of magnesium, silica, and calcium reflect an under prediction of solution pH, although the pH in our models is below that which would affect amorphous silica. Unfortunately, in our study, pH is

one of the most difficult parameters to predict because values at elevated temperature must be extrapolated to 25ºC to compare with the measured values. The measured and predicted pH are then subject to change due to possible mineral precipitation and equilibration with atmospheric CO_2(g) at room temperature. Furthermore, measured pH values in concentrated solutions are uncorrected and do not represent real H^+ activity. We have minimized the contribution of pH uncertainty to the observed discrepancy by constraining predicted pH by fitting the $\sum CO_2$(aq) concentration in leg 4, where we observed measurable concentrations. This yields a solution in equilibrium with atmospheric CO_2 and an initial pH of 7.5 at 95ºC. This is consistent with the experiment, because filtered laboratory air was continually passed over the solution as the waters evaporated, and because carbonate samples were stored in gas-tight vials eliminating exchange with atmospheric CO_2 at room temperature. We also assume that the undiluted, sealed samples taken for pH measurement did not re-equilibrate with atmospheric CO_2 as they cooled from 95ºC to room temperature. The good agreement between measured and predicted pH at lower ionic strengths in legs 1 and 2 supports these modeling constraints.

4.0 DISCUSSION

4.1 Chemical Divides

The important chemical divides that control the composition of brines formed from dilute sulfate type waters are halite, bassanite (or other calcium sulfates), magnesium silicate, amorphous silica, and possibly fluorite and brucite based on experimental results and model predictions. The early removal of fluoride from the starting solution is an important geochemical control for eliminating the evolution of a potentially corrosive fluoride containing brine. The precipitation of calcium as a calcium carbonate is not a major chemical divide for this solution. At 95ºC and atmospheric CO_2(g), carbonate is partitioned into the gas phase rather than the precipitation of calcium carbonate. The solution is below calcite solubility for most of the experiment. The precipitation of calcium as bassanite and magnesium as a magnesium silicate are important geochemical controls that limit the calcium and magnesium content in these brines. Additionally, the very low fluoride solubility limits chloride to be the most corrosive agent of Yucca Mountain sulfate type pore waters. High nitrate to chloride ratios of brines are known to limit susceptibility to localized corrosion of corrosion resistant materials such as the candidate waste package material.[18, 19] The brine contained a nitrate to chloride ratio of 0.2:1 at 99.97% evaporation. This ratio will increase with increasing evaporation because the chloride will be controlled by halite solubility, and nitrate will continue to concentrate until the solution reaches saturation with respect to nitratine ($NaNO_3$) and/or niter (KNO_3).

Although the $Ca:SO_4:HCO_3$ ternary diagrams do not capture all of the important chemical divides that affect the composition of Yucca Mountain pore waters, they can be used to categorize the types of brines that will form from the wide range of Yucca Mountain pore waters. Evaporation of dilute sulfate (this study), bicarbonate and calcium chloride[5] type Yucca Mountain waters evolve towards their respective sulfate, carbonate and calcium chloride brines indicated by their initial $Ca:SO_4:HCO_3$ ratios (Figure 2).

4.2 High Temperature Pitzer Model

The comparison of experimental results and model predictions of the evaporation of synthetic Topopah Spring Tuff pore water at 95ºC indicates that the current high-temperature Pitzer database used by the Yucca Mountain program adequately describes the chemical evolution of brines at elevated temperature for most species (Figure 3). In this section we discuss our results in light of the high temperature Pitzer ion interaction database that includes solubility products for solids. Appendix 1 lists temperature dependent Pitzer interaction parameters for binary and ternary reactions and Appendix 2 details the solubility products relevant to this work.

The Yucca Mountain Project high temperature Pitzer ion interaction database is the most comprehensive database available to account for the non-ideal behavior of highly concentrated electrolytes over a wide range of temperature (0 to 140ºC). The database was founded on the original variable-temperature Pitzer parameters[20, 21] supplemented by parameter data from several other sources[13, 22-32]. It also includes thermodynamic parameters converted from non-standard Pitzer equations from the published literature.[14] Temperature independent parameters based on 25ºC data are used for several parameters where temperature dependent data are lacking.[13] The database contains temperature dependent ion interaction parameters for most ion groups relevant to our experimental system at 95ºC. Exceptions include 25ºC models for potassium nitrate interactions and some calcium and magnesium ion interactions [13]; and 20 to 90ºC models for CO_2(aq) ion interactions.[26]. Substantial database and model validation has been performed[1], however, it is acknowledged that the results of any model are only as good as the input parameters and database used, and typically, improvements will always be made to bridge the gaps between experimental observations and model predictions.

4.2.1 Na^+, Cl^-, K^+, and NO_3^-

The excellent agreement between model prediction and experiment for sodium, chloride, potassium, and nitrate suggests that the high temperature Pitzer ion interaction database and halite solubility product adequately describes the non-ideal solution chemistry at high ionic strength and elevated temperature for these elements, as well as the halite solubility product. The agreement is expected for sodium and chloride because interaction parameters for binary and ternary ion groups are well defined as a function of temperature.[14, 21, 25, 27, 33, 34, 35]

The excellent agreement between prediction and experiment for potassium and nitrate suggests that Pitzer parameters for the K^+-NO_3^- ion interaction will yield accurate predictions of pore water concentrations in evaporating solutions despite being measured at 25ºC and applied to 95ºC systems. The reason for this is that high sodium to potassium, and chloride to nitrate mole ratios seen in our experiments may effectively mask any mismatch due to constant 25ºC parameters. Clearly, this is true for under saturated brines with respect to KNO_3 (niter) because Na^+-NO_3^- and K^+-Cl^- interactions will be more important than K^+-NO_3^- interactions in determining solution properties. However, when brines are saturated with niter (KNO_3), then K^+-NO_3^- interactions are more important. The extent that the constant temperature K^+-NO_3^- interaction parameter does not accurately predict behavior was shown in KNO_3-$NaNO_3$

deliquescence experiments at 90ºC. In solutions saturated with respect to niter/nitratine, they showed an under prediction of niter solubility by as much as 50%.[35]

4.2.2 Ca^{2+} and SO_4^{2-}

The discrepancy between experimental results and model prediction for dissolved calcium and sulfate concentrations observed in the high ionic strength solutions of leg 4 may be due to either the temperature dependent Ca^{2+}-SO_4^{2-} Pitzer parameters or an uncertainty in the physical nature of the calcium sulfate precipitate formed during the course of the experiment. The parameters in the Yucca Mountain database are derived from a refit of the Moller[20], and Greenberg and Moller[21] models, but without an explicit temperature dependent $CaSO_4$(aq) ion pair. To examine the ability of the high temperature Pitzer parameters to accurately predict calcium sulfate solubility, we compare model calculations to literature anhydrite and bassanite solubility in solutions of varying sodium chloride concentrations.[36,37,] The results are presented in Figure 5 and show agreement within 0.01 molal between predicted and measured anhydrite and bassanite solubility, which is similar to the agreement between measured and predicted calcium in our evaporation experiment, but it is as much as 7 times lower than the measured and predicted sulfate in our evaporation experiments.

The exact nature of the calcium sulfate solid phase formed in the experiment and controlling the solution concentrations of both calcium and sulfate may also contribute to the discrepancy between evaporation models and experiment. Gypsum changes rapidly to bassanite in contact with water at 97.5ºC[38] while bassanite is considered metastable and in turn is converted slowly to anhydrite at similar temperatures[39]. The gypsum-anhydrite transition temperature of 42ºC is known to increase in the presence of additional salts in solution. Recall, that both bassanite and anhydrite were identified by XRD at the end of the experimental evaporation. Clearly, our experimental conditions are such that gypsum-bassanite-anhydrite transitions may occur both during the evaporation experiment at 95ºC and during the drying of the final precipitates at 40ºC prior to XRD analysis. Our experimental calcium concentrations during the evaporation in leg 4 generally fall between those predicted by the presence of bassanite and anhydrite (Figure 5b). The $CaSO_4$ solubility comparison shown in Figure 5a is validated only to 6 molal, prior to the precipitation of halite. A theoretical solid solution composition with end members resembling both bassanite and anhydrite may be more appropriate in describing the nature of our evaporation solids.

4.2.3 ΣCO_2(aq) and pH

The prediction of solution pH is important because pH greatly affects the solubility of many carbonate and silicate phases. The Pitzer database contains parameters for several ion interactions that were derived from highly acidic or alkaline solutions (0 to >6 molal) that are not representative of the pH of natural solutions or brines ($4 < pH < 12$). In natural systems, the pH is strongly tied to the partial pressure of CO_2(g), as well as the dissociation of CO_2(aq) to HCO_3^- and CO_3^{2-}. He and Morse[26] derived Pitzer parameters for ion interactions involving CO_2(aq),

HCO_3^- and CO_3^{2-} in strong electrolytes containing sodium, potassium, calcium, magnesium, chloride and sulfate from calcite solubility experiments from 0 to 90ºC. While the parameters based on He and Morse[26] are incorporated into the Yucca Mountain Pitzer database, the Pitzer parameter temperature function embedded in the EQ3/6 code is not always consistent with published Pitzer data (e.g. too few or too many Pitzer parameters). Consequently, Pitzer data are required to be re-fit to be internally consistent with both the EQ3/6 code. As stated earlier, we measured only uncorrected pH values in our evaporation study and most measured carbonate concentrations fell below the analytical limit of detection.

To evaluate our ability to model H_2O-CO_2 systems, we utilized the equilibria between calcite, dissolved carbonate and pH. We compare model calculations with known literature calcite solubility data approached from undersaturation in 1 to 5 molal sodium chloride brines (with lesser concentrations of potassium, calcium, and sulfate) from 25 to 90ºC.[40, 41] We do not compare similar calcite seeded experiments approached from supersaturation because He and Morse[26] observed higher solubility, which they attributed to cation substitution in the precipitated calcite. The results are shown in Figure 6. At higher temperatures approaching those of our evaporation study, model calculations match calcite solubility to within 0.003 to 0.004 molal. Thus model calculations of pH and $\Sigma CO_2(aq)$ are reasonable reflections of the experimental equilibrium.

4.2.4 Mg and Si

The factor of two discrepancy between model and experiment for magnesium and silica solubility translates to absolute concentrations on the order of 0.01 molal for magnesium and only 10^{-5} molal for silica. This agreement suggests that the use of sepiolite and brucite ($Mg(OH)_2$) to model magnesium and silica solubility, and the high temperature Pitzer parameters are adequate for the evaporation of waters in a repository environment. Since precipitates formed in the synthesis of the initial solution were not carried over to evaporation studies, formation (and loss through precipitation) of magnesium and silica solids could result in a discrepancy between model and experimental results. Uncertainty in the sepiolite solubility product is well defined at temperatures less than 100ºC, with log K_{sp} = 24 (±0.3) at 95ºC ($Mg_4Si_6O_{15}(OH)_2 \bullet 4H_2O + 8H^+ = 4Mg^{2+} + 6SiO_2(aq) + 11H_2O$).[42] This translates to less than 10% uncertainty. Sepiolite has been observed as a likely control for the removal of magnesium and/or silica in other systems such as at Saline Valley, California (USA) that have a brine evolution similar to this experimental pore water.[43] It is doubtful that an amorphous magnesium silicate forms, because the model slightly over predicts magnesium and silica concentrations. The observed match between model and experiment also suggests that the suppression of talc is valid because its formation is thought to be kinetically unfavorable. However, additional studies are needed to identify the magnesium silicate phase that controls solubility.

The absolute over prediction of silica solubility is well within the uncertainty of Pitzer parameters in the high temperature database. We evaluate the Mg^{2+}-$SiO_2(aq)$ Pitzer parameters by comparing model calculations of $SiO_2(am)$ solubility data in magnesium and sodium containing electrolytes at 100ºC in Figure 7.[44, 45] Mg^{2+}-$SiO_2(aq)$ Pitzer parameters were initially derived from amorphous silica solubility measured in a range of electrolyte solutions [32, 44-46] in which parameter accuracy is limited by low silica concentrations and uncertainty in the chemical

potential for amorphous silica[32]. Model calculations in systems in which amorphous silica controls solubility (sepiolite is suppressed) slightly over-predict silica solubility by 0.001 molal on average. If sepiolite and amorphous silica are allowed to control silica solubility, then the scatter in the data noticeably increases to an average of 0.003 molal. These values are more than two orders of magnitude higher than the over-prediction observed in our evaporation study.

5.0 CONCLUSION

The assessment of water chemistry that may contact the waste containers and drip shields at the Yucca Mountain high-level radioactive waste repository in Nevada, USA requires the calculation of a wide range of water composition over 10,000 year time periods in an environment in which temperature and relative humidity will change as the repository heats up and cools down. Understanding and verifying the chemical divides that control brine composition as seepage water evaporates is important to placing boundaries on the corrosiveness of the chemical environment to waste package materials. The model data generated for this solution by EQ3/6 geochemical code and high temperature Pitzer database indicate that they can provide satisfactory predictions as compared to the experimental data in most cases. The water evolved towards a complex sulfate type brine that contained about 45 mol% Na, 40 mol % Cl, 9 mol% NO_3, 5 mol % K, and less than 1 mol % each of SO_4, Ca, Mg, $\sum CO_2(aq)$, F, and Si at a concentration factor of about 3500x. Minerals predicted to form include halite, anhydrite, bassanite, niter and nitratine in addition to fluoride, carbonate, sulfate and magnesium silicate precipitates. This work is of importance to the continued validation of the Pitzer ion-interaction parameter database and geochemical modeling used by the Yucca Mountain Project, and supports its adequate capabilities in predicting brine evolution in complex aqueous systems at elevated temperatures.

ACKNOWLEDGEMENTS

The authors would like to thank Brian Viani and Tom Wolery at LLNL for their guidance and discussion regarding X-ray diffraction data and thermodynamic modeling respectively and Kirk Staggs for his invaluable skills in making these experiments possible.

This work was performed under the auspices of the U.S. Department of Energy by the University of California Lawrence Livermore National Laboratory under contract No. W-7405-Eng-48.

REFERENCES

1 Bechtel SAIC Company, In-Drift Precipitates/Salts Model, Analysis Model Report ANL-EBS-MD-000045 Rev 01 ICN 01 (2004) Available at www.ocrwm.doe.gov/technical/amr.shtml. Accessed March 2005.

2 Eugster, H.P. and Hardie, L.A., Saline lakes, In: Lerman, A. (Ed.), Lakes: Chemistry, Geology, Physics. Springer-Verlag, New York, (1978).
3 Drever, J.I., The Geochemistry of Natural Waters: Surface and Groundwater Environments, 3rd Edition. Prentice Hall, New Jersey, (1997).
4 Eary, E.L., Predicting the effects of evapoconcentration on water quality in mine pit lakes. Journal of Geochemical Exploration, 64, 223 (1998).
5 Rosenberg, N.D., Gdowski, G. E., and Knauss K.G., Evaporative chemical evolution of natural waters at Yucca Mountain, Nevada. Applied Geochemistry, 16, 1231 (2001).

6 Yang, I. C., Rattray, G. W., Yu, P., Interpretation of Chemical and Isotopic Data from Boreholes in the Unsaturated Zone at Yucca Mountain, Nevada. USGS Water Resources Investigation Report 96-4058, US Geological survey, Denver, CO, (1996).
7 Peterman, Zell E., Marshall, Brian D., Geochemistry of pore water from densely welded Topopah Spring Tuff at Yucca Mountain, Nevada (abs): Geological Society of America Abstracts with Programs, v. 34, n. 6, p.308 (2002).
8 Bechtel SAIC Company, FY01 Supplemental Science and Performance Analysis, V. 1 Scientific Basis and Analyses, Report #TDR-MGR-MD-000007 REV 0, p. 6-56 to 6-59 (2001). Available at http://lsnnet.gov. Accessed March 2005.
9 Hardie, L.A. and Eugster, H. P., The evolution of closed-basin brines. Mineral Society Amer. Spec. Pap., 3, 273 (1970).
10 Li, J., Lowenstein, T. K., Blackburn, I. R.,. Responses of evaporite mineralogy to inflow water sources and climate during the past 100 k.y. in Death Valley, California. GSA Bulletin, 109, 1361 (1997).
11 Bates, R.G., Ion activity scales for use with selective ion-sensitive electrodes. Pure and Applied Chemistry, 36, 407 (1973).
12 Bechtel SAIC Company, EQ3/6, A software package for geochemical modeling of aqueous systems, v8.0, (2003), developed by Wolery, T.J. and Jarek, R.L. and available from Bechtel SAIC, STN: 10813-8.0-00.
13 Pitzer, K. S., Activity Coefficients in Electrolyte Solutions, 2nd edition. CRC Press, Boca Raton, (1991).
14 Rard, J.A. and Wijesinghe, A.M., Conversion of parameters between different variants of Pitzer's ion-interaction model, both with and without ionic strength dependent higher-order terms. Journal of Chemical Thermodynamics 35, 439 (2003).
15 Pulvirenti, A.L., Needham, K.M., Adel-Hadadi, M.A., Bishop, E.J., Barkatt, A., Marks, C.R., Gorman, J.A., Effects of Volatilization on Groundwater Chemistry. Materials Research Society Symposium Proceedings Vol.757, (2003).
16 Kent, D.B. and Kastner, M., Mg^{2+} removal in the system Mg^{2+}-amorphous SiO_2-H_2O by adsorption and Mg-hydroxysilicate precipitation. Geochimica et Cosmochimica Acta 49, 1123 (1985).
17 Rai, D., Felmy, A.R., Juracich, S.P., and Rao, F., Estimating the hydrogen ion concentration in concentrated NaCl and Na_2SO_4 electrolytes SAND94-1949 UC-721. Sandia National Laboratories, Albuquerque, NM, (1995).
18 Dunn, D.S. and Brossia, C.S., Assessment of passive and localized corrosion processes for alloy 22 as a high-level nuclear waste container material, Corrosion Paper No.02548, (2002).

19 Gordon, G.M., F.N. Speller Award Lecture: Corrosion Considerations Related to Permanent Disposal of High-Level Radioactive Waste. Corrosion, 58 (10), 811, (2002).
20 Moller, N., The prediction of mineral solubilities in natural waters: A chemical equilibrium model for the Na-Ca-Cl-SO_4-H_20 system, to high temperature and concentration. Geochimica et Cosmochimica Acta, 52, 821 (1988).
21 Greenberg, J.P. and Moller, N., The prediction of mineral solubilities in natural waters: A chemical equilibrium model for the Na-K-Ca-Cl-SO_4-H_2O system to high concentration from 0 to 250ºC. Geochimica et Cosmochimica Acta, 53, 2503 (1989).
22 Holmes, H.F. and Mesmer, R.E., Thermodynamic properties of aqueous solutions of the alkali metal chlorides to 250ºC. Journal of Physical Chemistry, 87, 1242 (1983).
23 Holmes, H.F. and Mesmer, R.E., An isopiestic study of aqueous solutions of the alkali metal bromides at elevated temperatures. Journal of Chemical Thermodynamics, 30, 723 (1998).
24 Holmes, H.F. and Mesmer, R.E., An isopiestic study of $\{(1-y)NaHSO_4 + yNa_2SO_4\}(aq)$ at elevated temperatures. Journal of Chemical Thermodynamics, 26, 581 (1994).
25 Pabalan, R.T. and Pitzer, K.S., Thermodynamics of concentrated electrolyte mixtures and the prediction of mineral solubilities to high temperatures for mixtures in the system Na-K-Mg-Cl-SO_4-OH-H_2O. Geochimica et Cosmochimica Acta, 51, 2429 (1987).
26 He, S. and Morse, J.W., The carbonic acid system and calcite solubility in aqueous Na-K-Ca-Mg-Cl-SO_4 solutions from 0 to 90ºC. Geochimica et Cosmochimica Acta, 57, 3533 (1993).
27 Holmes, H.F., Busey, R.H., Simonson, J.M., and Mesmer, R.E., The enthalpy of dilution of HCl(aq) to 648 K and 40 MPa. Journal of Chemical Thermodynamics, 19, 863 (1987).
28 Oakes, C.S. and Felmy, A.R., Thermodynamic properties of aqueous calcium nitrate $\{Ca(NO3)_2\}$ to the temperature 373 K including new enthalpy of dilution data. Journal of Chemical Thermodynamics, 32, 29 (2000).
29 Clegg, S.L., Milioto, S., and Palmer, D.A., Osmotic and activity coefficients of aqueous $(NH_4)_2SO_4$ as a function of temperature, and aqueous $(NH_4)_2SO_4$-H_2SO_4 mixtures at 298.15 K and 323.15 K. Journal of Chemical Engineering Data, 41, 455 (1996).
30 Thiessen, W.E. and Simonson, J.M., Enthalpy of dilution and the thermodynamics of NH_4Cl(aq) to 523 K and 35 MPa. Journal of Physical Chemistry, 94, 7794 (1990).
31 Clegg, S.L. and Brimblecombe, P., The solubility and activity coefficient of oxygen in salt solutions and brines. Geochimica et Cosmochimica Acta, 54, 3315 (1990).
32 Felmy, A.R., Schroeder, C.C., and Mason, M.J., A solubility model for amorphous silica in concentrated electrolytes. Presented at the Symposium of Scientific Issues Related to Safety and Treatment of Hanford Waste Tanks, August 21-26, Washington, D.C., 1994, PNL-SA-25345, (1994).
33 Archer, D. G., Thermodynamic properties of the $NaNO_3$+H_2O System. Journal of Physical Chemistry. Ref. Data, 29 (5), 1141 (2000).
34 Sterner, S.M., Felmy, A.R., Oakes, C.S., and Pitzer, K.S., International Journal of Thermophysics, 19, 3, 761 (1998).
35 Craig, L., Carroll, S., and Wolery, T., Deliquescence of NaCl-$NaNO_3$ and KNO_3-$NaNO_3$ salt mixtures at 90ºC. Water Rock Interaction Proceedings WRI-11 Vol.II, 1275 (2004).
36 Blount, C.W. and Dickson, F.W., The solubility of anhydrite (CaSO4) in NaCl-H2O from 100 to 450ºC and 1 to 1000 bars. Geochimica et Cosmochimica Acta, 33, 227 (1969).

37 Marshall, W.L., Slusher, R. and Jones, E.V., Solubility and thermodynamic relationships for $CaSO_4$ in NaCl-H_2O solutions from 40º to 200º C., 0 to 4 molal NaCl. J. Chem. Eng. Data, 9, 187 (1964).
38 Posnjak, E., The System $CaSO_4$-H_2O. American Journal of Science, 235, A, 247 (1938).
39 Partridge, E.. and White, A.H., The solubility of calcium sulfate from 0 to 200ºC. J. Amer. Chem. Soc, 51, 201 (1929).
40 He, S., Effects of solution composition, temperature and pressure on the carbonic acid system and calcite solubility in the system Na-K-Mg-Ca-HCl-SO_4-OH-HCO_3-CO_3-CO_2-H_2O. PhD Dissertation, Texas A&M University, (1992).
41 Lervson, A.I., Geology of Petroleum, 2nd edition. W.H Freeman, San Francisco, (1967).

42 Helgeson, H.C., Delany, J.M., Nesbitt, H.W., and Bird, D.K., Summary and critique of the thermodynamic properties of rock-forming minerals. Am. J. Sci., 278-A (1978).
43 Hardie, L.A., The origin of the Recent non-marine evaporite deposit of Saline Valley, Inyo County, California. Geochimica et Cosmochimica Acta, 22, 1279 (1968).
44 Marshall, W.L. and Chen, C.A., Amorphous silica solubilities V. Predictions of solubility behavior in aqueous mixed electrolyte solutions to 300ºC. Geochimica et Cosmochimica Acta, 46, 289 (1982).
45 Marshall, W.L. and Chen, C.A., Amorphous silica solubilities-VI. Postulated sulfate-silicic acid solution complex. Geochimica et Cosmochimica Acta, 46, 367 (1982).
46 Chen, C.A. and Marshall, W.L., Amorphous silica solubilities IV. Behavior in pure water and aqueous sodium chloride, sodium sulfate, magnesium chloride, and magnesium sulfate solutions up to 350ºC. Geochimica et Cosmochimica Acta, 46, 279 (1982).
47 Pabalan, R.T. and Pitzer, K.S., Thermodynamics of a NaOH(aq) in hydrothermal solutions. Geochimica et Cosmochimica Acta, 51, 829 (1987).
48 Harvie, C.E., Moller, N. and Weare, J.H., The prediction of mineral solubilities in natural waters: The Na-K-Mg-Ca-H-Cl-SO_4-OH-HCO_3-CO_3-CO_2-H_2O system to high ionic strengths at 25ºC, Geochimica et Cosmochimica Acta, 48, 723 (1984).
49 Barin, I. and Platzki, G., Thermochemical Data of Pure Substances (3rd Edition). New York, VCH, (1995).

Table 1. Starting and final compositions for the evaporation of a synthetic "sulfate type" Topopah Spring Tuff pore water.

	Leg 1 FEC 9 Molal[1] starting	Leg 1 FEC 9 molal 95ºC starting	Leg 1 FEC 9 molal, 95ºC final	Leg 2 FEC 12 molal 95ºC starting	Leg 2 FEC 12 molal, 95ºC final	Leg 3* FEC 13 molal 95ºC starting	Leg 3 FEC 13 molal, 95ºC final	Leg 4* FEC 14 molal 95ºC starting	Leg 4 FEC 14 molal, 95ºC final
PH[1]	9.65	na	7.15	7.60	7.32	7.69	na	8.08	6.97
F	5.94×10^{-5}	nd	nd	nd	nd	nd	nd	nd	nd
Ca	1.57×10^{-3}	1.25×10^{-3}	4.36×10^{-3}	4.69×10^{-3}	2.25×10^{-2}	2.17×10^{-2}	4.21×10^{-2}	4.06×10^{-2}	1.03×10^{-2}
Mg	1.01×10^{-3}	6.48×10^{-4}	5.58×10^{-4}	6.05×10^{-4}	4.52×10^{-3}	1.06×10^{-3}	6.43×10^{-3}	1.88×10^{-3}	9.02×10^{-3}
Na	2.84×10^{-3}	3.04×10^{-3}	9.23×10^{-3}	1.10×10^{-2}	1.05×10^{-1}	1.11×10^{-1}	1.15	1.12	7.42
SiO_2	1.39×10^{-3}	9.21×10^{-4}	1.15×10^{-3}	1.38×10^{-3}	7.91×10^{-3}	2.24×10^{-3}	6.32×10^{-3}	3.09×10^{-4}	1.89×10^{-5}
K	1.76×10^{-4}	1.63×10^{-4}	5.15×10^{-4}	5.82×10^{-4}	5.66×10^{-3}	6.54×10^{-3}	6.99×10^{-2}	7.89×10^{-2}	8.09×10^{-1}
Cl	3.26×10^{-3}	3.31×10^{-3}	1.00×10^{-2}	9.80×10^{-3}	9.80×10^{-2}	1.05×10^{-1}	9.93×10^{-1}	1.09	6.59
NO_3	3.53×10^{-4}	3.94×10^{-4}	1.15×10^{-3}	1.32×10^{-3}	1.12×10^{-2}	1.18×10^{-2}	1.29×10^{-1}	1.32×10^{-1}	1.42
SO_4	1.23×10^{-3}	1.85×10^{-3}	4.54×10^{-3}	4.64×10^{-3}	2.35×10^{-2}	2.24×10^{-2}	5.85×10^{-2}	5.80×10^{-2}	1.36×10^{-1}
HCO_3	7.93×10^{-4}	3.11×10^{-4}	nd	1.59×10^{-4}	nd	1.92×10^{-4}	nd	1.95×10^{-4}	2.66×10^{-4}

1. Measured at room temperature.

* Magnesium and silica precipitated from the solution at 25ºC. Initial gravimetric concentrations are Mg = 4.5×10^{-3} mol/kg-solution and Si = 7.8×10^{-3} mol/kg-solution for Leg3 and are Mg = 6.0×10^{-3} mol/kg-solution and Si = 5.9×10^{-3} mol/kg-solution for Leg4.

na = not analyzed, nd = not detected, detection limits: F=0.25ppm, HCO_3=1ppm

Table 2. Concentration (molal) of a synthetic "sulfate type" Topopah Spring Tuff pore water as it evaporated at 95ºC.

	SAMPLE	Concentration Factor	pH*	HCO_3^-	Ca	Mg	Si	Na	K	Cl	NO_3	SO_4
Leg 1	FEC9-1	1.00	na	3.11×10^{-4}	1.25×10^{-3}	6.48×10^{-4}	9.21×10^{-4}	3.04×10^{-3}	1.63×10^{-4}	3.31×10^{-3}	3.94×10^{-4}	1.85×10^{-3}
	FEC9-2	1.07	na	2.46×10^{-4}	1.64×10^{-3}	3.11×10^{-4}	6.27×10^{-4}	3.11×10^{-3}	1.73×10^{-4}	3.56×10^{-3}	3.97×10^{-4}	1.95×10^{-3}
	FEC9-3	1.23	na	1.16×10^{-4}	1.91×10^{-3}	2.56×10^{-4}	6.07×10^{-4}	3.68×10^{-3}	1.99×10^{-4}	4.06×10^{-3}	4.48×10^{-4}	2.23×10^{-3}
	FEC9-4	1.55	7.94	nd	2.31×10^{-3}	2.95×10^{-4}	6.97×10^{-4}	4.42×10^{-3}	2.46×10^{-4}	5.09×10^{-3}	5.27×10^{-4}	2.80×10^{-3}
	FEC9-5	2.08	7.18	nd	3.11×10^{-3}	3.86×10^{-4}	8.86×10^{-4}	5.93×10^{-3}	3.37×10^{-4}	6.97×10^{-3}	6.94×10^{-4}	3.74×10^{-3}
	FEC9-6	3.15	7.57	nd	4.36×10^{-3}	5.58×10^{-4}	1.15×10^{-3}	9.23×10^{-3}	5.15×10^{-4}	1.00×10^{-2}	1.15×10^{-3}	4.54×10^{-3}
Leg 2	FEC12-1	3.15	8.6	1.59×10^{-4}	4.69×10^{-3}	6.05×10^{-4}	1.38×10^{-3}	1.10×10^{-2}	5.82×10^{-4}	9.80×10^{-3}	1.32×10^{-3}	4.64×10^{-3}
	FEC12-2	3.44	8.29	nd	5.12×10^{-3}	6.05×10^{-4}	1.46×10^{-3}	1.20×10^{-2}	5.65×10^{-4}	1.08×10^{-2}	1.40×10^{-3}	5.12×10^{-3}
	FEC12-3	3.63	7.91	nd	5.43×10^{-3}	6.17×10^{-4}	1.51×10^{-3}	1.28×10^{-2}	6.70×10^{-4}	1.14×10^{-2}	1.45×10^{-3}	5.42×10^{-3}
	FEC12-4	4.23	7.87	nd	6.53×10^{-3}	7.08×10^{-4}	1.77×10^{-3}	1.53×10^{-2}	7.70×10^{-4}	1.37×10^{-2}	1.69×10^{-3}	6.46×10^{-3}
	FEC12-5	4.85	7.59	nd	7.49×10^{-3}	8.14×10^{-4}	2.05×10^{-3}	1.74×10^{-2}	8.91×10^{-4}	1.62×10^{-2}	1.92×10^{-3}	7.65×10^{-3}
	FEC12-6	5.93	7.19	nd	9.25×10^{-3}	9.95×10^{-4}	2.53×10^{-3}	2.16×10^{-2}	1.15×10^{-3}	1.91×10^{-2}	2.29×10^{-3}	9.00×10^{-3}
	FEC12-7	7.65	7.61	nd	1.17×10^{-2}	1.26×10^{-3}	3.18×10^{-3}	2.72×10^{-2}	1.42×10^{-3}	2.49×10^{-2}	2.92×10^{-3}	1.17×10^{-2}
	FEC12-8	11.79	7.47	nd	1.77×10^{-2}	1.92×10^{-3}	4.79×10^{-3}	4.14×10^{-2}	2.28×10^{-3}	3.79×10^{-2}	4.43×10^{-3}	1.77×10^{-2}
	FEC12-9	28.42	7.32	nd	2.25×10^{-2}	4.52×10^{-3}	7.91×10^{-3}	1.05×10^{-1}	5.66×10^{-3}	9.80×10^{-2}	1.12×10^{-2}	2.35×10^{-2}
Leg 3	FEC13-1	28.42	7.69	1.92×10^{-4}	2.17×10^{-2}	1.06×10^{-3}	2.24×10^{-3}	1.11×10^{-1}	6.54×10^{-3}	1.05×10^{-1}	1.18×10^{-2}	2.24×10^{-2}
	FEC13-2	38.63	7.07	nd	2.06×10^{-2}	8.99×10^{-4}	2.87×10^{-3}	1.37×10^{-1}	8.90×10^{-3}	1.29×10^{-1}	1.64×10^{-2}	2.28×10^{-2}
	FEC13-3	47.95	6.99	nd	2.04×10^{-2}	9.80×10^{-4}	3.38×10^{-3}	1.57×10^{-1}	1.27×10^{-2}	1.52×10^{-1}	2.00×10^{-2}	2.42×10^{-2}
	FEC13-4	64.87	6.4	nd	2.71×10^{-2}	1.54×10^{-3}	4.24×10^{-3}	2.37×10^{-1}	1.34×10^{-2}	2.00×10^{-1}	2.89×10^{-2}	2.80×10^{-2}
	FEC13-5	129.02	6.21	nd	2.91×10^{-2}	2.62×10^{-3}	6.41×10^{-3}	4.55×10^{-1}	2.55×10^{-2}	3.66×10^{-1}	4.59×10^{-2}	3.24×10^{-2}
	FEC13-6	187.64	6.34	nd	3.38×10^{-2}	3.52×10^{-3}	6.60×10^{-3}	6.18×10^{-1}	4.13×10^{-2}	5.46×10^{-1}	7.36×10^{-2}	4.27×10^{-2}
	FEC13-7	306.40	na	nd	4.21×10^{-2}	6.43×10^{-3}	6.32×10^{-3}	1.15×10^{0}	6.99×10^{-2}	9.93×10^{-1}	1.29×10^{-1}	5.85×10^{-2}
Leg 4	FEC14-1	306.40	8.076	1.95×10^{-4}	4.06×10^{-2}	1.88×10^{-3}	3.09×10^{-4}	1.12×10^{0}	7.89×10^{-2}	1.09×10^{0}	1.32×10^{-1}	5.80×10^{-2}
	FEC14-2	361.93	7.82	1.74×10^{-4}	4.27×10^{-2}	1.95×10^{-3}	1.98×10^{-4}	1.35×10^{0}	9.22×10^{-2}	1.28×10^{0}	1.54×10^{-1}	6.28×10^{-2}
	FEC14-3	409.63	7.476	1.67×10^{-4}	4.38×10^{-2}	2.10×10^{-3}	1.53×10^{-4}	1.52×10^{0}	1.05×10^{-1}	1.46×10^{0}	1.76×10^{-1}	6.67×10^{-2}
	FEC14-4	465.88	7.899	1.52×10^{-4}	4.51×10^{-2}	2.27×10^{-3}	1.25×10^{-4}	1.76×10^{0}	1.21×10^{-1}	1.68×10^{0}	2.00×10^{-1}	7.09×10^{-2}
	FEC14-5	632.48	7.772	1.39×10^{-4}	4.19×10^{-2}	2.81×10^{-3}	1.05×10^{-4}	2.37×10^{0}	1.62×10^{-1}	2.23×10^{0}	2.73×10^{-1}	7.24×10^{-2}
	FEC14-6	820.18	7.946	1.69×10^{-4}	3.89×10^{-2}	3.41×10^{-3}	8.62×10^{-5}	3.09×10^{0}	2.13×10^{-1}	2.90×10^{0}	3.51×10^{-1}	7.70×10^{-2}
	FEC14-7	1227.81	7.376	1.53×10^{-4}	2.82×10^{-2}	4.83×10^{-3}	6.16×10^{-5}	4.66×10^{0}	3.15×10^{-1}	4.40×10^{0}	5.26×10^{-1}	8.41×10^{-2}
	FEC14-8	1734.09	6.87	1.30×10^{-4}	1.94×10^{-2}	6.40×10^{-3}	4.65×10^{-5}	6.60×10^{0}	4.40×10^{-1}	6.20×10^{0}	7.44×10^{-1}	9.97×10^{-2}
	FEC14-9	2601.94	6.971	2.94×10^{-4}	1.23×10^{-2}	8.48×10^{-3}	3.12×10^{-5}	7.20×10^{0}	6.44×10^{-1}	6.61×10^{0}	1.09×10^{0}	1.28×10^{-1}
	FEC14-10	3389.64	7.322	2.66×10^{-4}	1.03×10^{-2}	9.02×10^{-3}	1.89×10^{-5}	7.42×10^{0}	8.09×10^{-1}	6.59×10^{0}	1.42×10^{0}	1.36×10^{-1}

* pH measured at room temperature, na = not analyzed, nd = not detected, detection limits: F=0.25ppm, HCO_3=1ppm

Table 3. Results of X-ray diffraction analysis of precipitates formed from complete evaporation.

	Leg 1 (Exp. FEC 9)	Leg 2 (Exp. FEC 12)	Leg 3 (Exp. FEC 13)	Leg 4 (Exp. FEC 14)
Halite (NaCl)	X	X	X	X
Anhydrite ($CaSO_4$)	X	X	X	X
Bassanite ($2CaSO_4 \cdot H_2O$)		X		X
Niter (KNO_3)				X
Nitratine ($NaNO_3$)				X

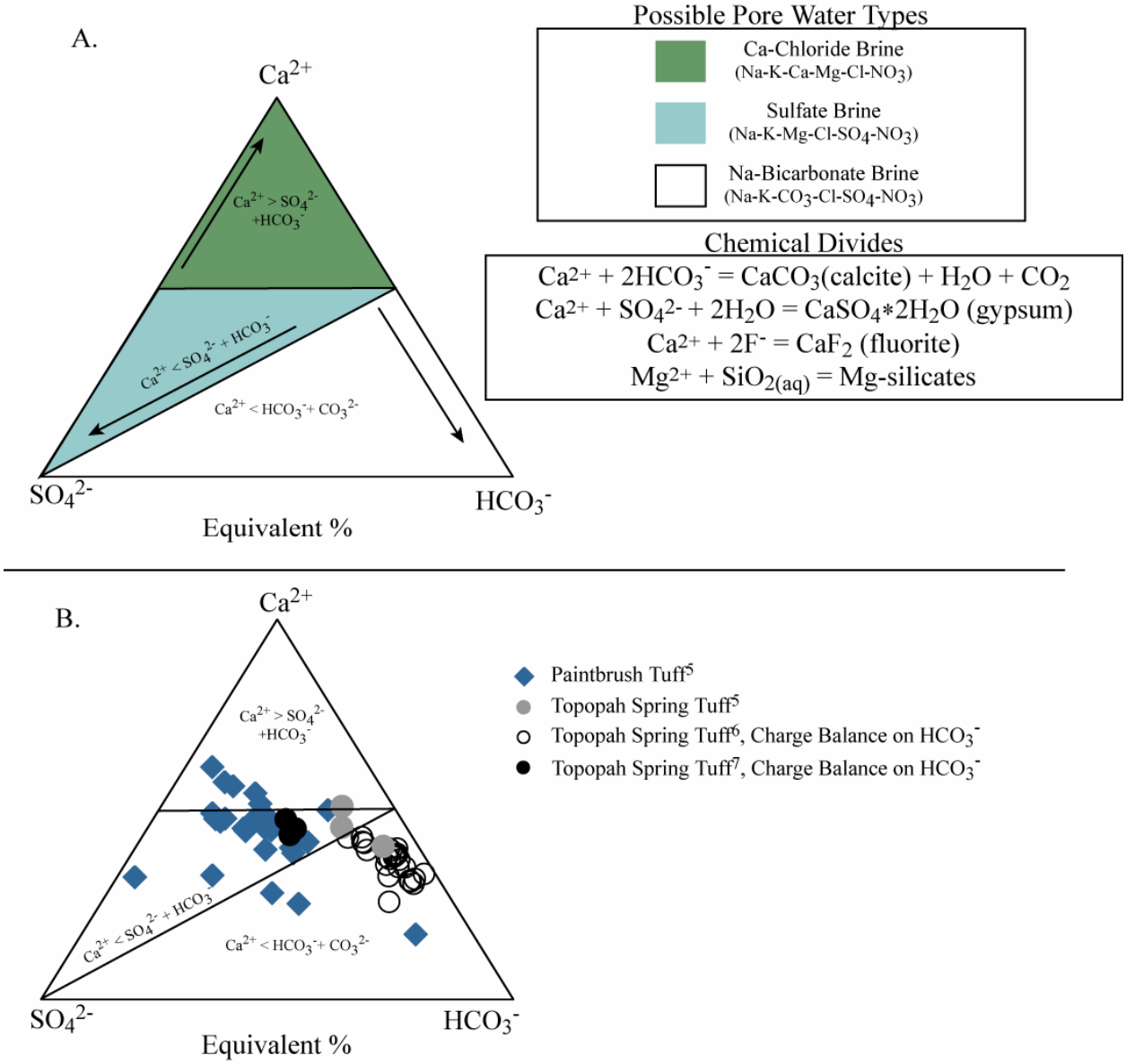

Figure 1. A. Calcium carbonate and calcium sulfate chemical divides for evaporation of dilute waters. B. Yucca Mountain, NV pore waters as measured.

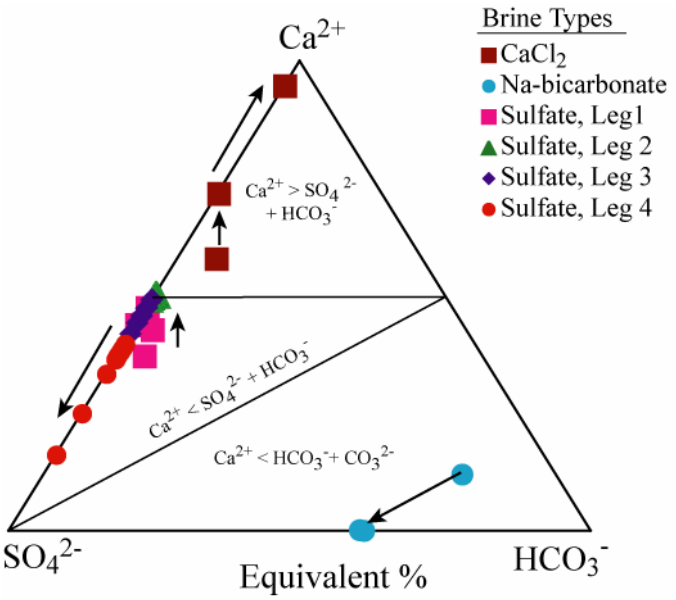

Figure 2. Chemical evolution of dilute calcium chloride (synthetic Topopah Spring tuff porewater[5]), Na-bicarbonate (synthetic J-13 groundwater[5]), and sulfate (synthetic Topopah Spring tuff porewater, this study) waters upon evaporation.

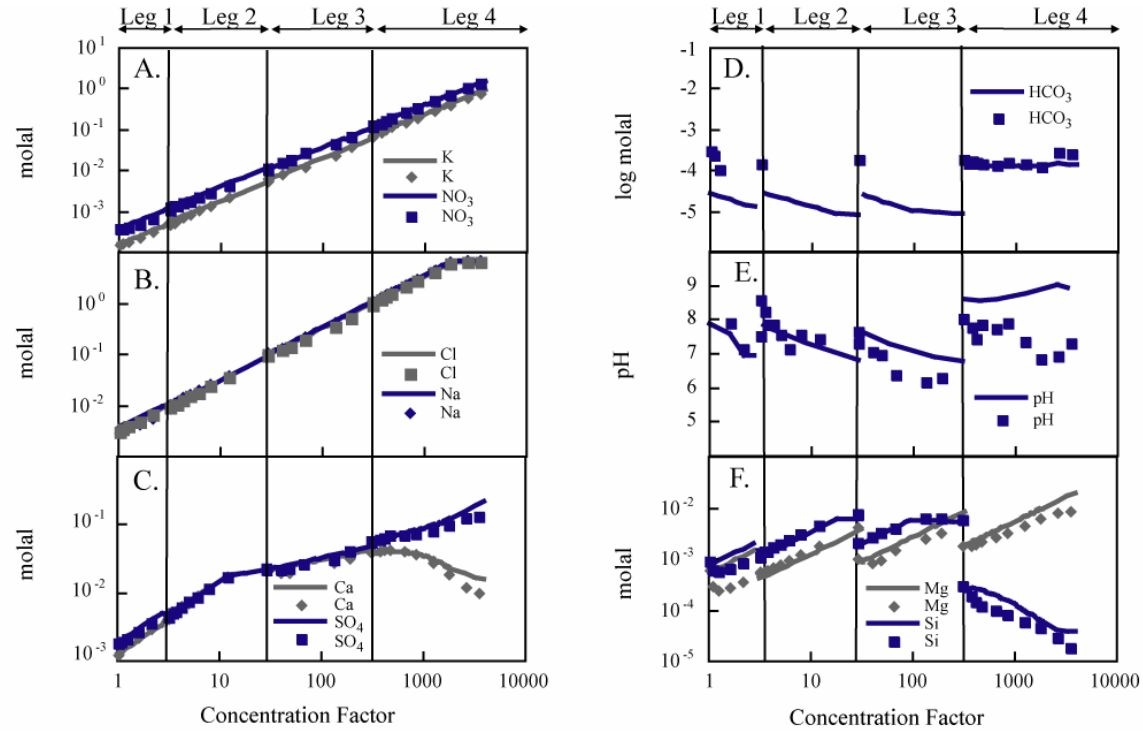

Figure 3. Evaporation of dilute sulfate water based on a Topopah Spring tuff porewater chemistry. Comparison of experimental and model solution concentrations vs. concentration factor. Symbols indicate experimental data and lines indicate model data.

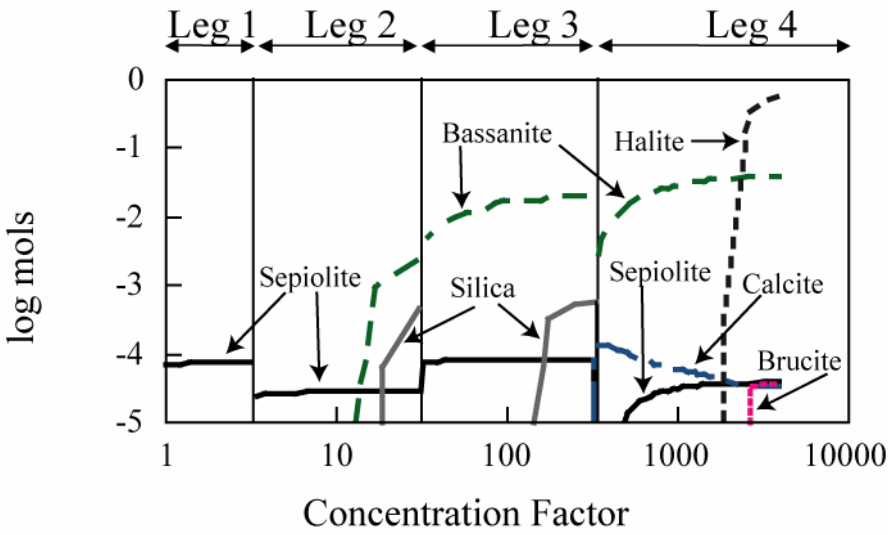

Figure 4. Evaporation of dilute sulfate water based on a Topopah Spring tuff porewater chemistry. Predicted mineral amounts vs. concentration factor.

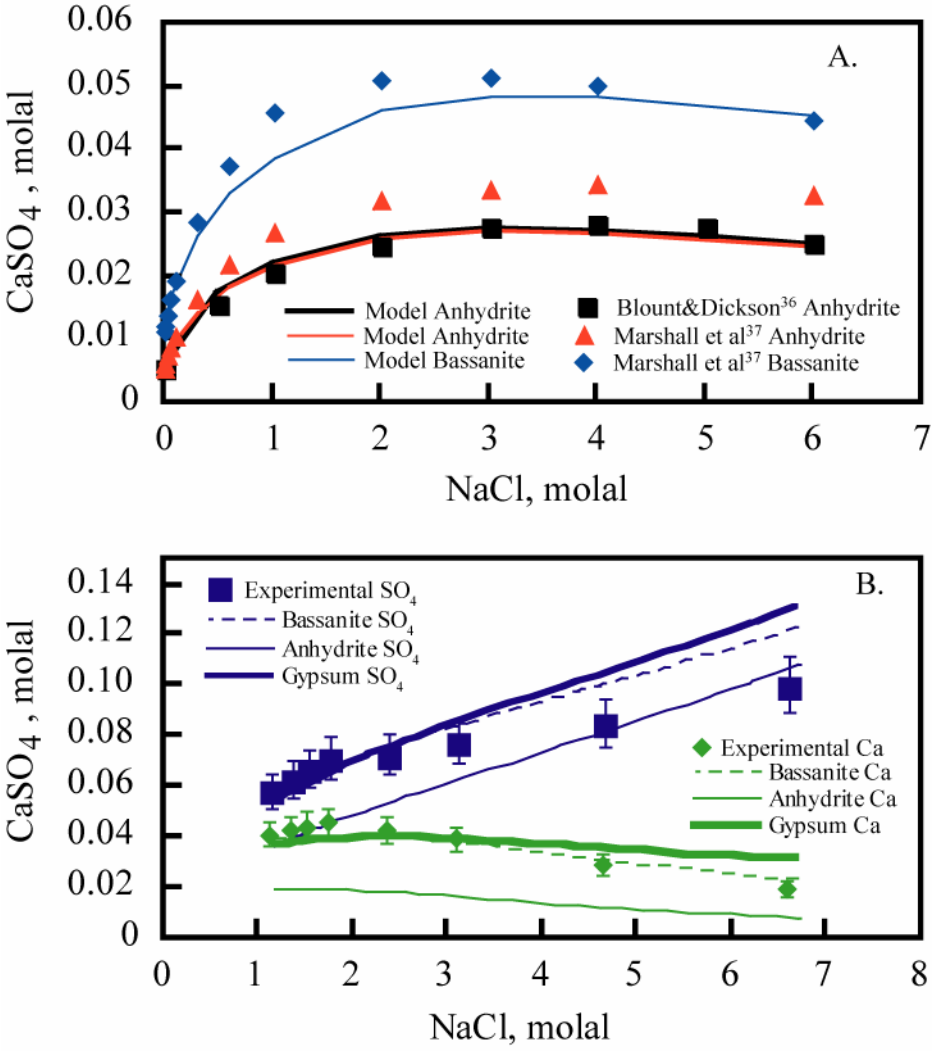

Figure 5. A. Comparison of literature and calculated anhydrite and bassanite solubility data. Literature values were only obtained up to 6 molal sodium, therefore our calcium sulfate validation is limited to this upper value. B. Comparison of modeled calcium and sulfate concentrations using bassanite, anhydrite and gypsum as the solubility controlling mineral phase and leg 4 calcium and sulfate concentrations prior to modeled halite formation.

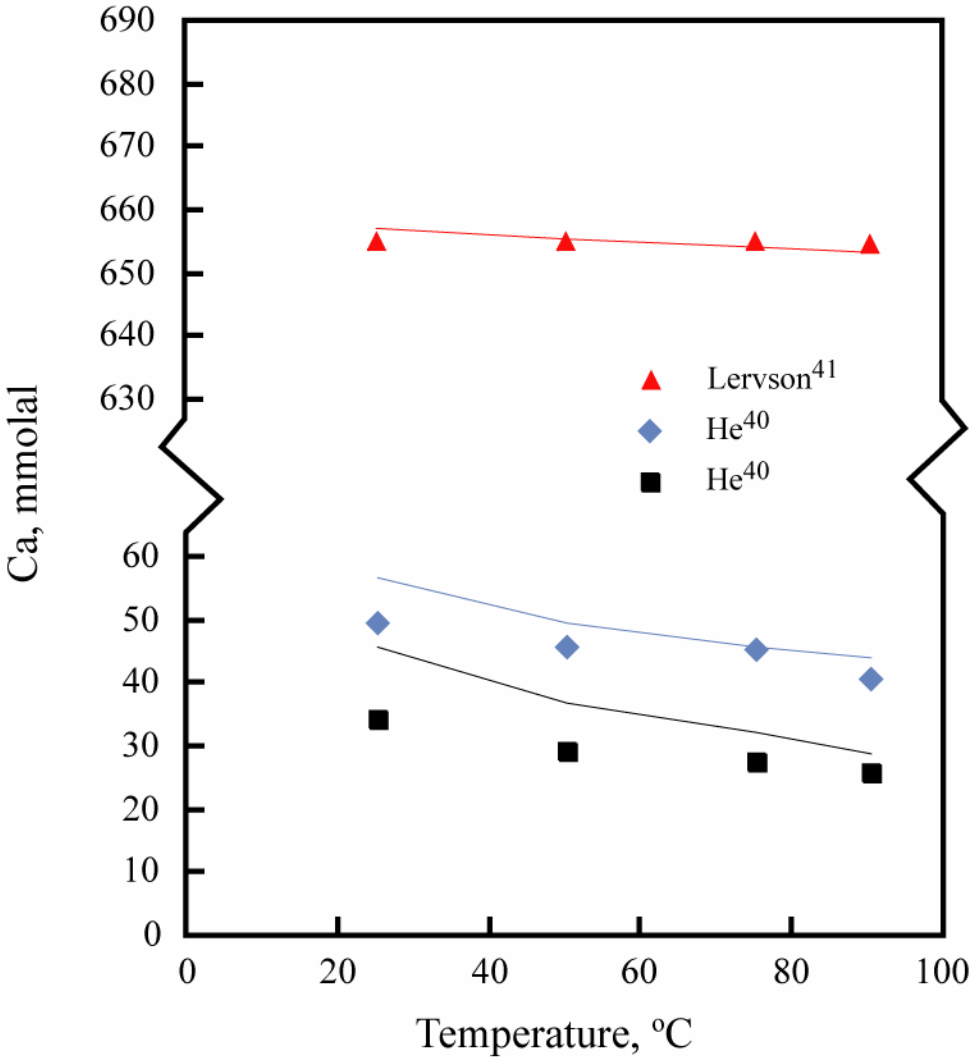

Figure 6. Comparison of model data to literature calcite solubility data approached from undersaturation in synthetic brines[26]. Lines represent LLNL model and symbols represent He[40] and Lervson[41] experimental data.

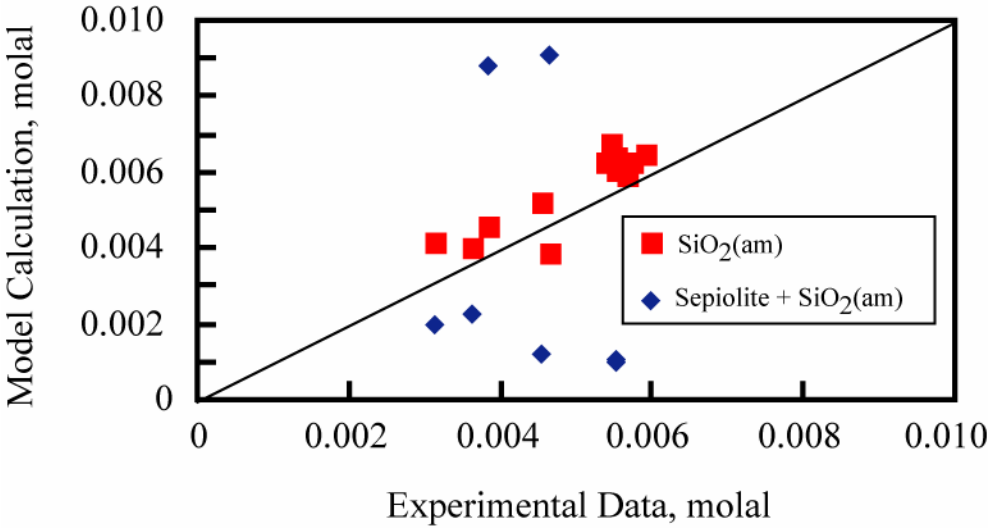

Figure 7. Comparison of silica solubility data in $MgCl_2$ and NaCl electrolytes at 100ºC[46] with predicted model calculations using the high temperature Pitzer ion interaction data base. Note that the smaller number of data plotted in the calculations, where both sepiolite and amorphous silica are allowed to control solubility, reflects the $MgCl_2$ electrolytes only.

Appendix 1. Temperature dependence of Pitzer interaction parameters. 25ºC-centric equation used to derive parameters: $\chi_{(T)} = a_1 + a_2[\{1/T\} - \{1/298.15\}] + a_3 \ln\{T/298.15\} + a_4\{T - 298.15\}$.

		Pitzer Interaction Parameters					
Ion Interactions		**Coefficients**	**a_1**	**a_2**	**a_3**	**a_4**	**Reference**
Ca^{++}	Cl^-	$\beta^{(0)}_{MX}$	4.46×10^{-1}	2.21×10^{2}	1.61×10^{-11}	2.28×10^{-4}	Sterner et al[34]
		$\beta^{(1)}_{MX}$	-1.66x10	-8.83×10^{3}	7.10×10^{-11}	-2.49×10^{-2}	
		$\beta^{(2)}_{MX}$	0.00	0.00	0.00	0.00	
		C^{ϕ}_{MX}	-1.73×10^{-2}	-1.30×10^{1}	-3.87×10^{-13}	-3.15×10^{-5}	
Ca^{++}	HCO_3^-	$\beta^{(0)}_{MX}$	4.00×10^{-1}	0.00	0.00	0.00	Pitzer[13]
		$\beta^{(1)}_{MX}$	2.98	0.00	0.00	0.00	
		$\beta^{(2)}_{MX}$	0.00	0.00	0.00	0.00	
		C^{ϕ}_{MX}	0.00	0.00	0.00	0.00	
Ca^{++}	HSO_4^-	$\beta^{(0)}_{MX}$	2.15×10^{-1}	0.00	0.00	0.00	Pitzer[13]
		$\beta^{(1)}_{MX}$	2.53	0.00	0.00	0.00	
		$\beta^{(2)}_{MX}$	0.00	0.00	0.00	0.00	
		C^{ϕ}_{MX}	0.00	0.00	0.00	0.00	
Ca^{++}	NO_3^-	$\beta^{(0)}_{MX}$	1.48×10^{-1}	-4.88×10^{1}	-7.47×10^{-2}	-1.70×10^{-4}	Oakes&Felmy[28]
		$\beta^{(1)}_{MX}$	2.44	-2.24×10^{4}	-9.93×10^{1}	1.19×10^{-1}	
		$\beta^{(2)}_{MX}$	0.00	0.00	0.00	0.00	
		C^{ϕ}_{MX}	-4.12×10^{-3}	-1.79×10^{1}	-1.19×10^{-1}	1.87×10^{-4}	
Ca^{++}	SO_4^{--}	$\beta^{(0)}_{MX}$	1.50×10^{-1}	0.00	0.00	0.00	Greenberg&Moller[21]
		$\beta^{(1)}_{MX}$	3.00	0.00	0.00	0.00	
		$\beta^{(2)}_{MX}$	0.00	0.00	0.00	0.00	
		C^{ϕ}_{MX}	0.00	0.00	0.00	0.00	
H^+	Cl^-	$\beta^{(0)}_{MX}$	1.77×10^{-1}	-3.35×10^{1}	-2.62×10^{-1}	1.26×10^{-4}	Holmes et al[27]
		$\beta^{(1)}_{MX}$	2.93×10^{-1}	3.40×10^{3}	1.98×10^{1}	-2.79×10^{-2}	
		$\beta^{(2)}_{MX}$	0.00	0.00	0.00	0.00	
		C^{ϕ}_{MX}	3.62×10^{-4}	-2.91×10^{-11}	0.00	-3.04×10^{-5}	
H^+	HSO_4^-	$\beta^{(0)}_{MX}$	2.09×10^{-1}	1.05×10^{3}	5.96	-8.78×10^{-3}	Holmes&Mesmer[24]
		$\beta^{(1)}_{MX}$	4.41×10^{-1}	2.96×10^{2}	2.37	-4.63×10^{-3}	
		$\beta^{(2)}_{MX}$	0.00	0.00	0.00	0.00	
		C^{ϕ}_{MX}	0.00	0.00	0.00	0.00	
H^+	NO_3^-	$\beta^{(0)}_{MX}$	1.26×10^{-1}	5.60×10^{2}	4.92	-9.95×10^{-3}	Felmy et al[32]
		$\beta^{(1)}_{MX}$	2.88×10^{-1}	2.71×10^{-7}	1.59×10^{-9}	1.34×10^{-3}	
		$\beta^{(2)}_{MX}$	0.00	0.00	0.00	0.00	
		C^{ϕ}_{MX}	-5.60×10^{-3}	-6.58	-5.77×10^{-2}	1.10×10^{-4}	
H^+	SO_4^{--}	$\beta^{(0)}_{MX}$	9.86×10^{-2}	-6.70×10^{3}	-4.17×10^{1}	6.37×10^{-2}	Pabalan&Pitzer[47]
		$\beta^{(1)}_{MX}$	0.00	0.00	0.00	0.00	
		$\beta^{(2)}_{MX}$	0.00	0.00	0.00	0.00	
		C^{ϕ}_{MX}	5.93×10^{-2}	-3.03×10^{3}	-1.61×10^{1}	2.02×10^{-2}	
K^+	Cl^-	$\beta^{(0)}_{MX}$	4.78×10^{-2}	-3.43×10^{2}	-1.38	1.34×10^{-3}	Greenberg&Moller[21]
		$\beta^{(1)}_{MX}$	2.16×10^{-1}	-5.76×10^{2}	-2.88	4.64×10^{-3}	
		$\beta^{(2)}_{MX}$	0.00	0.00	0.00	0.00	
		C^{ϕ}_{MX}	-7.49×10^{-4}	3.65×10^{1}	1.48×10^{-1}	-1.47×10^{-4}	
K^+	CO_3^{--}	$\beta^{(0)}_{MX}$	1.29×10^{-1}	0.00	0.00	0.00	Pitzer[13]
		$\beta^{(1)}_{MX}$	1.43	0.00	0.00	0.00	

		$\beta^{(2)}_{MX}$	0.00	0.00	0.00	0.00	
		C^{ϕ}_{MX}	4.99×10^{-4}	0.00	0.00	0.00	
K^+	F^-	$\beta^{(0)}_{MX}$	8.09×10^{-2}	0.00	0.00	0.00	Pitzer[13]
		$\beta^{(1)}_{MX}$	2.02×10^{-1}	0.00	0.00	0.00	
		$\beta^{(2)}_{MX}$	0.00	0.00	0.00	0.00	
		C^{ϕ}_{MX}	9.30×10^{-4}	0.00	0.00	0.00	
K^+	HCO_3^-	$\beta^{(0)}_{MX}$	-1.07×10^{-2}	0.00	0.00	0.00	Pitzer[13]
		$\beta^{(1)}_{MX}$	4.78×10^{-2}	0.00	0.00	0.00	
		$\beta^{(2)}_{MX}$	0.00	0.00	0.00	0.00	
		C^{ϕ}_{MX}	0.00	0.00	0.00	0.00	
K^+	HSO_4^-	$\beta^{(0)}_{MX}$	-3.00×10^{-4}	0.00	0.00	0.00	Pitzer[13]
		$\beta^{(1)}_{MX}$	1.74×10^{-1}	0.00	0.00	0.00	
		$\beta^{(2)}_{MX}$	0.00	0.00	0.00	0.00	
		C^{ϕ}_{MX}	0.00	0.00	0.00	0.00	
K^+	NO_3^-	$\beta^{(0)}_{MX}$	-8.16×10^{-2}	0.00	0.00	0.00	Pitzer[13]
		$\beta^{(1)}_{MX}$	4.94×10^{-2}	0.00	0.00	0.00	
		$\beta^{(2)}_{MX}$	0.00	0.00	0.00	0.00	
		C^{ϕ}_{MX}	6.60×10^{-3}	0.00	0.00	0.00	
K^+	OH^-	$\beta^{(0)}_{MX}$	1.30×10^{-1}	0.00	0.00	0.00	Pitzer[13]
		$\beta^{(1)}_{MX}$	3.20×10^{-1}	0.00	0.00	0.00	
		$\beta^{(2)}_{MX}$	0.00	0.00	0.00	0.00	
		C^{ϕ}_{MX}	4.10×10^{-3}	0.00	0.00	0.00	
K^+	SO_4^{--}	$\beta^{(0)}_{MX}$	5.55×10^{-2}	-1.42×10^{3}	-6.75	8.27×10^{-3}	Greenberg&Moller[21]
		$\beta^{(1)}_{MX}$	7.96×10^{-1}	2.07×10^{3}	2.33×10^{-10}	2.36×10^{-2}	
		$\beta^{(2)}_{MX}$	0.00	0.00	0.00	0.00	
		C^{ϕ}_{MX}	-1.88×10^{-2}	0.00	9.09×10^{-13}	-2.66×10^{-15}	
Mg^{++}	Cl^-	$\beta^{(0)}_{MX}$	3.51×10^{-1}	-6.56×10^{1}	-5.25×10^{-1}	4.47×10^{-4}	Pabalan&Pitzer[47]
		$\beta^{(1)}_{MX}$	1.65	-2.87×10^{3}	-2.30×10^{1}	4.95×10^{-2}	
		$\beta^{(2)}_{MX}$	0.00	0.00	0.00	0.00	
		C^{ϕ}_{MX}	6.53×10^{-3}	-2.67×10^{1}	-2.14×10^{-1}	3.11×10^{-4}	
Mg^{++}	HCO_3^-	$\beta^{(0)}_{MX}$	3.30×10^{-2}	0.00	0.00	0.00	Pitzer[13]
		$\beta^{(1)}_{MX}$	8.50×10^{-1}	0.00	0.00	0.00	
		$\beta^{(2)}_{MX}$	0.00	0.00	0.00	0.00	
		C^{ϕ}_{MX}	0.00	0.00	0.00	0.00	
Mg^{++}	HSO_4^-	$\beta^{(0)}_{MX}$	4.75×10^{-1}	0.00	0.00	0.00	Pitzer[13]
		$\beta^{(1)}_{MX}$	1.73	0.00	0.00	0.00	
		$\beta^{(2)}_{MX}$	0.00	0.00	0.00	0.00	
		C^{ϕ}_{MX}	0.00	0.00	0.00	0.00	
Mg^{++}	NO_3^-	$\beta^{(0)}_{MX}$	3.67×10^{-1}	0.00	0.00	0.00	Pitzer[13]
		$\beta^{(1)}_{MX}$	1.58	0.00	0.00	0.00	
		$\beta^{(2)}_{MX}$	0.00	0.00	0.00	0.00	
		C^{ϕ}_{MX}	-2.06×10^{-2}	0.00	0.00	0.00	
Mg^{++}	SO_4^{--}	$\beta^{(0)}_{MX}$	2.23×10^{-1}	-5.69×10^{3}	-3.28×10^{1}	4.73×10^{-2}	Pabalan&Pitzer[47]
		$\beta^{(1)}_{MX}$	3.38	-2.32×10^{4}	-1.39×10^{2}	2.18×10^{-1}	
		$\beta^{(2)}_{MX}$	-3.53×10^{1}	2.17×10^{6}	1.40×10^{4}	-2.28×10^{1}	
		C^{ϕ}_{MX}	2.44×10^{-2}	1.89×10^{3}	1.08×10^{1}	-1.56×10^{-2}	
$MgOH^+$	Cl^-	$\beta^{(0)}_{MX}$	-1.00×10^{-1}	0.00	0.00	0.00	Pitzer[13]
		$\beta^{(1)}_{MX}$	1.66	0.00	0.00	0.00	
		$\beta^{(2)}_{MX}$	0.00	0.00	0.00	0.00	
		C^{ϕ}_{MX}	0.00	0.00	0.00	0.00	

Na^+	Cl^-	$\beta^{(0)}_{MX}$	$7.46x10^{-2}$	$-4.71x10^{2}$	-1.85	$1.66x10^{-3}$	Greenberg&Moller[21]
		$\beta^{(1)}_{MX}$	$2.75x10^{-1}$	$-5.21x10^{2}$	-2.88	$4.71x10^{-3}$	
		$\beta^{(2)}_{MX}$	0.00	0.00	0.00	0.00	
		C^{ϕ}_{MX}	$1.54x10^{-3}$	$4.81x10^{1}$	$1.75x10^{-1}$	$-1.56x10^{-4}$	
Na^+	CO_3^{--}	$\beta^{(0)}_{MX}$	$3.62x10^{-2}$	$1.11x10^{3}$	$1.12x10^{1}$	$-2.33x10^{-2}$	He&Morse[26]
		$\beta^{(1)}_{MX}$	1.51	$4.41x10^{3}$	$4.46x10^{1}$	$-9.99x10^{-2}$	
		$\beta^{(2)}_{MX}$	0.00	0.00	0.00	0.00	
		C^{ϕ}_{MX}	$5.20x10^{-3}$	0.00	0.00	$8.88x10^{-16}$	
Na^+	F^-	$\beta^{(0)}_{MX}$	$2.15x10^{-2}$	0.00	0.00	0.00	Pitzer[13]
		$\beta^{(1)}_{MX}$	$2.11x10^{-1}$	0.00	0.00	0.00	
		$\beta^{(2)}_{MX}$	0.00	0.00	0.00	0.00	
		C^{ϕ}_{MX}	0.00	0.00	0.00	0.00	
Na^+	HCO_3^-	$\beta^{(0)}_{MX}$	$2.80x10^{-2}$	$6.83x10^{2}$	6.90	$-1.45x10^{-2}$	He&Morse[26]
		$\beta^{(1)}_{MX}$	$4.40x10^{-2}$	$1.13x10^{3}$	$1.14x10^{1}$	$-2.45x10^{-2}$	
		$\beta^{(2)}_{MX}$	0.00	0.00	0.00	0.00	
		C^{ϕ}_{MX}	0.00	0.00	0.00	0.00	
Na^+	HSO_4^-	$\beta^{(0)}_{MX}$	$7.34x10^{-2}$	$5.26x10^{1}$	$4.21x10^{-1}$	$-8.21x10^{-4}$	Holmes&Mesmer[24]
		$\beta^{(1)}_{MX}$	$3.00x10^{-1}$	$4.70x10^{3}$	$2.68x10^{1}$	$-3.74x10^{-2}$	
		$\beta^{(2)}_{MX}$	0.00	0.00	0.00	0.00	
		C^{ϕ}_{MX}	$-4.62x10^{-3}$	$-5.82x10^{-11}$	$-2.27x10^{-13}$	$6.82x10^{-6}$	
Na^+	NO_3^-	$\beta^{(0)}_{MX}$	$3.57x10^{-3}$	$-7.03x10^{2}$	-3.35	$3.98x10^{-3}$	Archer[33]
		$\beta^{(1)}_{MX}$	$2.32x10^{-1}$	$-2.73x10^{3}$	$-1.30x10^{1}$	$2.07x10^{-2}$	
		$\beta^{(2)}_{MX}$	0.00	0.00	0.00	0.00	
		C^{ϕ}_{MX}	$-4.15x10^{-5}$	$6.48x10^{1}$	$3.18x10^{-1}$	$-3.84x10^{-4}$	
Na^+	OH^-	$\beta^{(0)}_{MX}$	$8.83x10^{-2}$	$-1.20x10^{3}$	-6.11	$7.43x10^{-3}$	He&Morse[26]
		$\beta^{(1)}_{MX}$	$2.44x10^{-1}$	$1.63x10^{3}$	9.48	$-1.16x10^{-2}$	
		$\beta^{(2)}_{MX}$	0.00	0.00	0.00	0.00	
		C^{ϕ}_{MX}	$4.00x10^{-3}$	$8.82x10^{1}$	$4.07x10^{-1}$	$-4.76x10^{-4}$	
Na^+	SO_4^{--}	$\beta^{(0)}_{MX}$	$1.21x10^{-2}$	$-2.19x10^{3}$	$-1.01x10^{1}$	$1.20x10^{-2}$	Greenberg&Moller[21]
		$\beta^{(1)}_{MX}$	1.12	$-1.27x10^{4}$	$-6.72x10^{1}$	$8.91x10^{-2}$	
		$\beta^{(2)}_{MX}$	0.00	0.00	0.00	0.00	
		C^{ϕ}_{MX}	$6.57x10^{-3}$	$3.39x10^{2}$	1.48	$-1.64x10^{-3}$	
Ca^{++}	H^+	${}^{S}\theta_{MM'}$	$9.20x10^{-2}$	0.00	0.00	0.00	Pitzer[13]
Ca^{++}	K^+	${}^{S}\theta_{MM'}$	$1.16x10^{-1}$	$9.31x10^{-10}$	0.00	$1.42x10^{-14}$	Greenberg&Moller[21]
Ca^{++}	Na^+	${}^{S}\theta_{MM'}$	$5.00x10^{-2}$	$1.86x10^{-9}$	$7.28x10^{-12}$	0.00	Greenberg&Moller[21]
Ca^{++}	Mg^{++}	${}^{S}\theta_{MM'}$	$7.00x10^{-3}$	0.00	0.00	0.00	Pitzer[13]
H^+	K^+	${}^{S}\theta_{MM'}$	$5.00x10^{-3}$	0.00	0.00	0.00	Pitzer[13]
H^+	Mg^{++}	${}^{S}\theta_{MM'}$	$1.00x10^{-1}$	0.00	0.00	0.00	Pitzer[13]
H^+	Na^+	${}^{S}\theta_{MM'}$	$3.60x10^{-2}$	0.00	0.00	0.00	Pitzer[13]
K^+	Mg^{++}	${}^{S}\theta_{MM'}$	0.00	0.00	0.00	0.00	Pabalan&Pitzer[47]
K^+	Na^+	${}^{S}\theta_{MM'}$	$-3.20x10^{-3}$	$1.40x10^{1}$	$9.09x10^{-13}$	$-2.66x10^{-15}$	Greenberg&Moller[21]
Mg^{++}	Na^+	${}^{S}\theta_{MM'}$	$7.00x10^{-2}$	0.00	0.00	0.00	Pitzer[13]
Cl^-	CO_3^{--}	${}^{S}\theta_{XX'}$	$-2.00x10^{-2}$	0.00	0.00	0.00	Pitzer[13]
Cl^-	HCO_3^-	${}^{S}\theta_{XX'}$	$3.00x10^{-2}$	0.00	0.00	0.00	Pitzer[13]
Cl^-	HSO_4^-	${}^{S}\theta_{XX'}$	$-6.00x10^{-3}$	0.00	0.00	0.00	Pitzer[13]
Cl^-	NO_3^-	${}^{S}\theta_{XX'}$	$1.60x10^{-2}$	0.00	0.00	0.00	Pitzer[13]
Cl^-	OH^-	${}^{S}\theta_{XX'}$	$-5.00x10^{-2}$	0.00	0.00	0.00	Pabalan&Pitzer [47]
Cl^-	SO_4^{--}	${}^{S}\theta_{XX'}$	$7.03x10^{-2}$	$1.83x10^{2}$	1.33	$-2.33x10^{-3}$	Greenberg&Moller[21]
CO_3^{--}	HCO_3^-	${}^{S}\theta_{XX'}$	$-4.00x10^{-2}$	0.00	0.00	0.00	Pitzer[13]
CO_3^{--}	OH^-	${}^{S}\theta_{XX'}$	$1.00x10^{-1}$	0.00	0.00	0.00	Pitzer[13]

CO_3^{--}	SO_4^{--}	${}^S\theta_{XX'}$	2.00×10^{-2}	0.00	0.00	0.00	Pitzer[13]
HCO_3^-	SO_4^{--}	${}^S\theta_{XX'}$	1.00×10^{-2}	0.00	0.00	0.00	Pitzer[13]
HSO_4^-	SO_4^{--}	${}^S\theta_{XX'}$	-1.17×10^{-1}	-3.09×10^{3}	-1.40×10^{1}	1.54×10^{-2}	Holmes&Mesmer[24]
OH^-	SO_4^{--}	${}^S\theta_{XX'}$	-1.30×10^{-2}	0.00	0.00	0.00	Pabalan&Pitzer [47]
CO_2(aq)	Ca^{++}	${}^S\lambda_{NM}$	1.98×10^{-1}	-6.51×10^{4}	-4.03×10^{2}	6.18×10^{-1}	He&Morse[26]
CO_2(aq)	H^+	${}^S\lambda_{NM}$	0.00	0.00	0.00	0.00	He&Morse[26]
CO_2(aq)	K^+	${}^S\lambda_{NM}$	4.58×10^{-2}	1.37×10^{4}	8.36×10^{1}	-1.28×10^{-1}	He&Morse[26]
CO_2(aq)	Mg^{++}	${}^S\lambda_{NM}$	1.95×10^{-1}	-3.96×10^{3}	-3.17×10^{1}	5.70×10^{-2}	He&Morse[26]
CO_2(aq)	Na^+	${}^S\lambda_{NM}$	7.75×10^{-2}	-1.92×10^{4}	-1.17×10^{2}	1.75×10^{-1}	He&Morse[26]
SiO_2(aq)	H^+	${}^S\lambda_{NM}$	0.00	0.00	0.00	0.00	Felmy et al[32]
SiO_2(aq)	Mg^{++}	${}^S\lambda_{NM}$	8.21×10^{-2}	-3.83×10^{-9}	-2.33×10^{-11}	-1.81×10^{-3}	Felmy et al[32]
SiO_2(aq)	Na^+	${}^S\lambda_{NM}$	-7.89×10^{-2}	-1.44×10^{-7}	-8.64×10^{-10}	1.19×10^{-4}	Felmy et al[32]
CO_2(aq)	Cl^-	${}^S\lambda_{NX}$	2.02×10^{-2}	5.08×10^{3}	3.01×10^{1}	-4.47×10^{-2}	He&Morse[26]
CO_2(aq)	HSO_4^-	${}^S\lambda_{NX}$	-3.00×10^{-3}	0.00	0.00	0.00	He&Morse[26]
CO_2(aq)	SO_4^{--}	${}^S\lambda_{NX}$	1.39×10^{-1}	4.99×10^{4}	3.09×10^{2}	-4.55×10^{-1}	He&Morse[26]
SiO_2(aq)	Cl^-	${}^S\lambda_{NX}$	1.42×10^{-1}	1.67×10^{2}	1.51	-3.22×10^{-3}	Felmy et al[32]
SiO_2(aq)	NO_3^-	${}^S\lambda_{NX}$	1.34×10^{-1}	6.30×10^{3}	3.55×10^{1}	-5.02×10^{-2}	Felmy et al[32]
SiO_2(aq)	SO_4^{--}	${}^S\lambda_{NX}$	7.76×10^{-2}	1.56×10^{-7}	9.33×10^{-10}	5.53×10^{-4}	Felmy et al[32]
Ca^{++} K^+	Cl^-	$\psi_{MM'X}$	-4.32×10^{-2}	-2.71×10^{1}	-3.64×10^{-12}	3.55×10^{-15}	Greenberg&Moller[21]
Ca^{++} Na^+	Cl^-	$\psi_{MM'X}$	-3.00×10^{-3}	0.00	1.14×10^{-13}	-6.66×10^{-16}	Greenberg&Moller[21]
Ca^{++} Na^+	SO_4^{--}	$\psi_{MM'X}$	-1.20×10^{-2}	0.00	4.55×10^{-13}	-2.66×10^{-15}	Greenberg&Moller[21]
K^+ Mg^{++}	Cl^-	$\psi_{MM'X}$	-2.20×10^{-2}	-1.43×10^{1}	0.00	0.00	Pabalan&Pitzer[47]
K^+ Na^+	Cl^-	$\psi_{MM'X}$	-3.69×10^{-3}	-5.10	-3.41×10^{-13}	6.66×10^{-16}	Greenberg&Moller[21]
K^+ Na^+	SO_4^{--}	$\psi_{MM'X}$	7.32×10^{-3}	-7.16×10^{1}	-3.94×10^{-1}	6.07×10^{-4}	Greenberg&Moller[21]
Mg^{++} Na^+	Cl^-	$\psi_{MM'X}$	-1.20×10^{-2}	-9.51	0.00	0.00	Pabalan&Pitzer[47]
Ca^{++} Cl^-	SO_4^{--}	$\psi_{MXX'}$	-1.80×10^{-2}	-6.98×10^{-10}	-2.73×10^{-12}	1.78×10^{-15}	Greenberg&Moller[21]
K^+ Cl^-	SO_4^{--}	$\psi_{MXX'}$	-1.62×10^{-3}	3.76×10^{1}	2.90×10^{-12}	2.85×10^{-4}	Greenberg&Moller[21]
H^+ HSO_4^-	SO_4^{--}	$\psi_{MXX'}$	0.00	0.00	0.00	0.00	Holmes&Mesmer[24]
Mg^{++} Cl^-	SO_4^{--}	$\psi_{MXX'}$	-7.96×10^{-3}	3.26×10^{1}	0.00	0.00	Pabalan&Pitzer[47]
Na^+ Cl^-	OH^-	$\psi_{MXX'}$	-6.01×10^{-3}	-9.93	0.00	0.00	Pabalan&Pitzer[47]
Na^+ Cl^-	SO_4^{--}	$\psi_{MXX'}$	-9.09×10^{-3}	-7.86×10^{1}	-5.52×10^{-1}	9.46×10^{-4}	Greenberg&Moller[21]
Na^+ HSO_4^-	SO_4^{--}	$\psi_{MXX'}$	1.44×10^{-2}	2.58×10^{2}	1.16	-1.26×10^{-3}	Holmes&Mesmer[24]
Na^+ OH^-	SO_4^{--}	$\psi_{MXX'}$	-9.10×10^{-3}	-1.17×10^{1}	0.00	0.00	Pabalan&Pitzer[47]
CO_2(aq)	Ca^{++} Cl^-	ζ_{NMX}	-1.61×10^{-2}	6.25×10^{3}	3.90×10^{1}	-6.04×10^{-2}	He&Morse[26]
CO_2(aq)	H^+ Cl^-	ζ_{NMX}	-4.65×10^{-3}	-1.31×10^{3}	-7.26	9.96×10^{-3}	He&Morse[26]
CO_2(aq)	H^+ SO_4^{--}	ζ_{NMX}	0.00	0.00	0.00	0.00	He&Morse[26]
CO_2(aq)	K^+ Cl^-	ζ_{NMX}	-1.27×10^{-2}	-9.33×10^{3}	-5.65×10^{1}	8.56×10^{-2}	He&Morse[26]
CO_2(aq)	K^+ SO_4^{--}	ζ_{NMX}	-4.10×10^{-4}	-1.12×10^{5}	-6.84×10^{2}	1.04	He&Morse[26]
CO_2(aq)	Mg^{++} Cl^-	ζ_{NMX}	-1.53×10^{-2}	-3.32×10^{3}	-1.97×10^{1}	2.94×10^{-2}	He&Morse[26]
CO_2(aq)	Mg^{++} SO_4^{--}	ζ_{NMX}	-9.28×10^{-2}	-6.09×10^{4}	-3.64×10^{2}	5.44×10^{-1}	He&Morse[26]
CO_2(aq)	Na^+ Cl^-	ζ_{NMX}	-5.50×10^{-4}	-3.97×10^{3}	-2.44×10^{1}	3.73×10^{-2}	He&Morse[26]
CO_2(aq)	Na^+ SO_4^{--}	ζ_{NMX}	-3.73×10^{-2}	-8.84×10^{3}	-5.48×10^{1}	8.49×10^{-2}	He&Morse[26]
SiO_2(aq)	H^+ NO_3^-	ζ_{NMX}	-3.30×10^{-3}	0.00	0.00	0.00	Felmy et al[32]
SiO_2(aq)	Mg^{++} Cl^-	ζ_{NMX}	-5.15×10^{-2}	1.50×10^{-8}	8.99×10^{-11}	5.94×10^{-4}	Felmy et al[32]
SiO_2(aq)	Na^+ Cl^-	ζ_{NMX}	-8.48×10^{-15}	-1.84×10^{-8}	-1.11×10^{-10}	-2.00×10^{-4}	Felmy et al[32]

Appendix 2. Log K temperature grid.

		log K Temperature Grid				
Mineral Name	**Mineral Formula**	**0°C**	**25°C**	**60°C**	**100°C**	**Reference**
Anhydrite	$CaSO_4$	-4.1258	-4.3193	-4.7307	-5.3507	Greenberg&Moller[21]
Aragonite	$CaCO_3$	2.3715	1.9931	1.4762	0.9179	Wolery&Jarek[12]
Arcanite	K_2SO_4	-2.1629	-1.7916	-1.4973	-1.397	Greenberg&Moller[21]
Artinite	$Mg_2CO_3(OH)_2:3H_2O$	21.7371	19.656	17.2642	15.1018	Wolery&Jarek[12]
Brucite	$Mg(OH)_2$	18.0898	16.298	14.2674	12.4514	Wolery&Jarek[12]
Burkeite	$Na_6CO_3(SO_4)_2$	No_Data	9.5671	No_Data	No_Data	Harvie et al[48]
Calcite	$CaCO_3$	2.2257	1.8487	1.333	0.7743	Wolery&Jarek[12]
Fluorite	CaF_2	-10.3098	-10.0371	-9.9067	-9.967	Wolery&Jarek[12]
Glaserite	$NaK_3(SO_4)_2$	No_Data	-3.8027	No_Data	No_Data	Harvie et al[48]
Glauberite	$Na_2Ca(SO_4)_2$	-4.7768	-5.1827	-5.7677	-6.5632	Greenberg&Moller[21]
Gypsum	$CaSO_4:2H_2O$	-4.5436	-4.5199	-4.6536	-4.9448	Greenberg&Moller[21]
Halite	NaCl	1.5012	1.5857	1.6084	1.569	Greenberg&Moller[21]
Hemihydrate	$2CaSO_4:H_2O$	-3.4301	-3.7773	-4.2698	-4.9372	Greenberg&Moller[21]
Huntite	$CaMg_3(CO_3)_4$	12.9081	10.301	7.0008	3.6895	Wolery&Jarek[12]
Kieserite	$MgSO_4:H_2O$	0.72	-0.0239	-1.0716	-2.2058	Pabalan&Pitzer[47]
Labile_Salt	$Na_2Ca_5(SO_4)_6:3H_2O$	18.2726	8.4195	6.7359	7.3639	Greenberg&Moller[21]
Magnesite	$MgCO_3$	2.9734	2.2936	1.4383	0.5875	Wolery&Jarek[12]
Natrite	Na_2CO_3	11.6028	10.984	10.2336	9.5237	Barin&Platzki[49]
Niter	KNO_3	-0.8418	-0.2344	0.3772	0.8541	Barin/Platzki 1995
Pentasalt	$K_2Ca_5(SO_4)_6:H_2O$	-23.9466	-24.5549	-26.5842	-29.0537	Greenberg&Moller[21]
Quartz	SiO_2	-4.1605	-3.7501	-3.3553	-3.0132	Wolery&Jarek[12]
Sellaite	MgF_2	-9.2699	-9.3939	-9.7091	-10.1577	Barin&Platzki[49]
Sepiolite	$Mg_4Si_6O_{15}(OH)_2:6H_2O$	32.3876	30.4439	27.171	23.8968	Wolery&Jarek[12]
Amorphous Silica	SiO_2	-3.124	-2.7136	-2.4067	-2.1843	Wolery&Jarek[12]
Nitratine (Soda Niter)	$NaNO_3$	0.7192	1.1009	1.4544	1.6902	Barin&Platzki[49]
Sylvite	KCl	0.6012	0.9148	1.1871	1.3418	Greenberg&Moller[21]
Syngenite	$K_2Ca(SO_4)2:H_2O$	-7.5463	-7.2618	-7.152	-7.2929	Greenberg&Moller[21]
Talc	$Mg_3Si_4O_{10}(OH)_2$	25.0261	22.1646	18.6126	15.3725	Wolery&Jarek[12]
Thenardite	Na_2SO_4	-0.1329	-0.2547	-0.4272	-0.6877	Greenberg&Moller[21]
Foshagite	$Ca_4Si_3O_9(OH)_2:0.5H_2O$	72.8341	66.691	59.4664	52.8906	Wolery&Jarek[12]
Gyrolite	$Ca_2Si_3O_7(OH)_2:1.5H_2O$	25.3869	23.6797	21.5505	19.6199	Wolery&Jarek[12]
Hillebrandite	$Ca_2SiO_3(OH)_2:0.17H_2O$	40.4592	37.0757	33.142	29.565	Wolery&Jarek[12]
Okenite	$CaSi_2O_4(OH)_2:H_2O$	11.4698	10.8948	10.147	9.5024	Wolery&Jarek[12]
Plombierite	$Ca_5Si_6H_{11}O_{22.5}$	69.8789	65.3842	59.9716	55.1602	Wolery&Jarek[12]
Riversideite	$Ca_5H_2(SiO_3)_6:2H_2O$	76.6335	70.6194	63.3144	56.6105	Wolery&Jarek[12]
Tobermorite	$5CaO:6SiO_2:5.5H_2O$	72.5004	67.1518	60.6578	54.7498	Wolery&Jarek[12]
Xonotlite	$Ca_6Si_6O_{17}(OH)_2$	102.0247	93.3664	82.9922	73.4523	Wolery&Jarek[12]